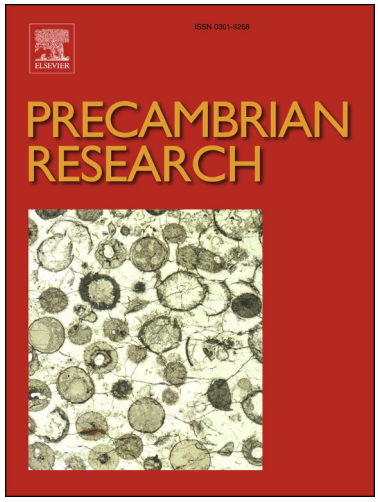

The petrogenesis of the Neoarchean Kukuluma Intrusive Complex, NW Tanzania

S.D. Kwelwa, I.V. Sanislav, P.H.G.M. Dirks, T. Blenkinsop, S.L. Kolling

PII: S0301-9268(17)30447-3
DOI: https://doi.org/10.1016/j.precamres.2017.12.021
Reference: PRECAM 4966

To appear in: *Precambrian Research*

Received Date: 1 August 2017
Revised Date: 4 October 2017
Accepted Date: 4 December 2017

Please cite this article as: S.D. Kwelwa, I.V. Sanislav, P.H.G.M. Dirks, T. Blenkinsop, S.L. Kolling, The petrogenesis of the Neoarchean Kukuluma Intrusive Complex, NW Tanzania, *Precambrian Research* (2017), doi: https://doi.org/10.1016/j.precamres.2017.12.021

The petrogenesis of the Neoarchean Kukuluma Intrusive Complex, NW Tanzania

S. D. Kwelwa[1, 2], I. V. Sanislav[1]*, P. H. G. M. Dirks[1], T. Blenkinsop[3], S. L. Kolling[2]

[1]*Economic Geology Research Centre (EGRU) and Department of Earth and Oceans, James Cook University, Townsville, 4011, QLD, Australia; e-mail: ioan.sanislav@jcu.edu.au; phone: (+61) 07 4781 3293; fax: (+61) 07 4781 5581*

[2]*Geita Gold Mine, Geita, P.O. Box 532, Geita Region, Tanzania*

[3] *School of Earth & Ocean Sciences, Cardiff University, Cardiff CF10 3AT, United Kingdom*

Abstract

The Kukuluma Intrusive Complex (KIC) is a late Archean igneous complex, dominated by monzonite and diorite with subordinated granodiorite. The monzonite and the diorite suites have low silica content ($SiO_2 \leq$ 62 wt%), moderate Mg# ($Mg\#_{average}$ = 49), high Sr/Y ($Sr/Y_{average}$ = 79) and high La/Yb ($La/Yb_{average}$ = 56) ratios, and strongly fractionated (La_n/Yb_n = 9 to 69) REE patterns. Their moderate Ni ($Ni_{average}$= 50 ppm), Cr ($Cr_{average}$= 85 ppm), variable Cr/Ni ratio (0.65-3.56) and low TiO_2 ($TiO_{2average}$= 0.5 wt%) indicate little to no interaction with the peridotitic mantle. For most major elements (Al_2O_3, FeO_t, Na_2O, TiO_2 and P_2O_5) the monzonite and the diorite suites display subparallel trends for the same SiO_2 content indicating they represent distinct melts. Intrusions belonging to the diorite suite have high Na_2O ($Na_2O_{average}$ = 4.2 wt %), Dy/Yb_n ($Dy/Yb_{n\text{-}average}$ = 1.6), a positive Sr anomaly and uncorrelated Nb/La and Zr/Sm ratios suggesting derivation from partial melting of garnet-bearing amphibolite. Intrusions belonging to the monzonite suite have higher Na_2O

23 ($Na2O_{average}$ = 5.61 wt %), Dy/Yb_n ($Dy/Yb_{n\text{-}average}$ = 2.21), a negative Sr anomaly and
24 correlated Nb/La and Zr/Sm ratios consistent with derivation from partial melting of eclogite
25 with residual rutile. Small variations in the Th/U ratio and near chondritic/MORB average
26 values ($Th/U_{monzonite}$ = 3.65; $Th/U_{diorite}$ = 2.92) are inconsistent with a subducting slab
27 signature, and it is proposed that the monzonite and the diorite suites of the KIC formed by
28 partial melting of garnet-bearing, lower mafic crust of an oceanic plateau. The granodiorite
29 suite has lower Mg# ($Mg\#_{average}$ = 41), moderately fractionated REE, low Sr/Y ($Sr/Y_{average}$ =
30 20), La/Yb ($La/Yb_{average}$ = 15), Dy/Yb_n ($DyYb_{n\text{-}average}$= 1.24) and small negative Eu anomalies
31 suggesting derivation from partial melting of amphibolite and plagioclase fractionation. Near-
32 MORB Th/U ($Th/U_{average}$ = 2.92) and Zr/Sm ($Zr/Sm_{average}$ = 30.21) ratios are consistent with
33 intracrustal melting of amphibolite.

34 Archean rocks with an "adakitic" geochemical signature have been used to argue in
35 favour of a plate tectonics regime in the Archean. The results presented here suggest that
36 tectonic models for the Tanzania Craton, which invoke a subduction-related setting for all
37 greenstone belts may need revision.

38

39 ## Introduction

40 The geochemical signature of intermediate to felsic rocks with fractionated REE
41 patterns and high Sr/Y and La/Yb ratios has been interpreted to indicate melt derivation from
42 a subducted slab at amphibolite to eclogite facies conditions (Defant and Drummond, 1990;
43 Drummond and Defant, 1990). Their particular geochemical signature, including a high Mg#
44 (molecular (Mg/Mg+Fe) x100) and enriched large-ion lithophile elements (LILE) were
45 interpreted to represent different degrees of interaction between slab melts and mantle
46 peridotite in the mantle wedge (e.g. Kay, 1978; Tatsumi and Ishizaka, 1981; Shirey and

Hanson, 1984; Stern et al., 1989; Defant and Drummond, 1990; Drummond and Defant, 1990; Tatsumi, 2006; Moyen, 2009; Castillo, 2012). Arc rocks with similar geochemical signatures, including andesite, dacite, sodic rhyolite and their plutonic equivalents, were grouped under the term "adakites" by Defant and Drummond (1990) implying they share a specific petrogenetic history, namely, melting of the subducted slab. Another class of rocks sharing similar petrogenetic processes (e.g. melting of mantle peridotite metasomatised by subduction fluids/melts) and geochemically similar to adakites includes the high-Mg andesites or sanukitoids (e.g. Tatsumi and Ishizaka, 1981; Shirey and Hanson, 1984; Tatsumi, 2006; Tatsumi, 2008), and the crustal contaminated sanukitoids of South India described as "Closepet-type" granites (Jayanada et al., 1995).

Both adakites and sanukitoids are derived from melting of a metamorphosed, garnet-bearing, mafic igneous rock protolith (e.g. Thorkelson and Breitsprecher, 2005). In the case of sanukitoids this probably involved melting of a metasomatised mantle wedge, and in the case of adakites the subducting slab, but the important message is that both suites are generally interpreted as imparting a subduction signature. Martin et al. (2005) subdivided adakites into two groups, low-silica adakites (LSA) and high-silica adakites (HSA), corresponding to distinct petrogenetic processes. In this subdivision the petrogenesis of LSA involves melting of subduction modified peridotite as originally proposed by Defant and Drummond (1990). In contrast, the HSA are proposed to be analogues of the late Archean tonalite-trondhjemite-granodiorite (TTG) magmas and derived from partial melts of subducted basaltic crust in the garnet stability field, which reacted with peridotite during ascent (Martin et al., 2005). Archean rocks with an "adakitic" geochemical signature have been used to argue in favour of a plate tectonics regime in the Archean (e.g. Martin, 1999; Polat and Kerrich, 2001; Manya et al., 2007; Manykyamba et al., 2007; Mohan et al., 2013; Kwelwa et al., 2013).

Alternative models for rocks with an "adakitic' signature have been proposed, and involve fractional crystallization in the garnet stability field (e.g. Kamber et al., 2002; Macpherson et al., 2006; Richard and Kerrich, 2007; Rooney et al., 2011), by melting of thickened mafic lower crust (e.g. Atherton and Petford, 1993; Rudnick, 1995; Wang et al., 2005), or through the interaction of delaminated eclogitic lower crust with the underlying mantle (e.g. Bedard et al., 2003; Tuloch and Kimbrough, 2003; Gao et al., 2004; Wang et al., 2005; Goss et al. 2011). Since most of the continental crust was formed in the Archean (e.g. Taylor and Mclennan, 1995; Tatsumi, 2008; Hacker et al., 2015) and the Archean rock record is dominated by rocks with an adakite-like (TTG's; e.g. Condie, 2005; Moyen, 2011; Moyen and Martin, 2012) geochemical signature, understanding the petrogenetic processes that resulted in the formation of rocks with an adakitic signature in the Archean is essential. This is particularly important for the late Archean period when major shifts in the composition of the TTG suites are interpreted to reflect fundamental changes in global tectonics (e.g. Condie, 2005; Martin et al., 2010; Moyen and Martin, 2012; Condie, 2014). In this contribution we present major and trace element geochemical data from the Kukuluma Intrusive Complex (KIC) that intruded the Neoarchean Geita Greenstone Belt of NW Tanzania and discuss the petrogenesis of the KIC, and the implications of this for the tectonic evolution of the Geita Greenstone Belt.

Regional geology

From a geological perspective, the Tanzania Craton was initially divided in three major litho-stratigraphic units: the Dodoman, the Nyanzian and the Kavirondian Supergroups (e.g. Stockley, 1936; Quennel et al., 1956; Harpum, 1970; Gabert, 1990). The Dodoman was interpreted to represent the basement to the Nyanzian, while the Kavirondian unconformably overlays the Nyanzian. The Dodoman consists of high-grade mafic and felsic granulite with

subordinate lower-grade schist and thin slivers of greenstone; the Nyanzian consists of mafic and felsic volcanics, ironstone, tuff and epiclastic sediments, while the Kavirondian consists of conglomerate, quartzite, grit, sandstone and siltstone. Borg and Krogh (1999) have shown that migmatitic gneisses, dated at 2680±3 Ma, that occur in the northern part of the Tanzania Craton are much younger than the Dodoman age units (interpreted to be ≥ 3000 Ma in age), and, therefore, cannot represent basement units. This was later confirmed by Chamberlain and Tosdal (2017), Kabete et al (2012) and Sanislav et al. (2014), who reviewed the existing geochronological data for the entire Tanzania Craton and concluded that there is no evidence of Dodoman age rock units in the northern half of the Tanzania Craton. Kabete et al. (2012), based on geophysical interpretation and limited field observations, divided the Tanzania Craton into a series of NW trending, shear-zone bounded accretionary terranes; they subdivided northern Tanzania (Fig. 1) into the Lake Nyanza Superterrane, Mwanza-Lake Eyasi Superterrane and the East Lake Victoria Superterrane.

The geology of the northern half of the Tanzania Craton is dominated by granite, gneiss and greenstone belts. Borg and Shackleton (1997) identified six greenstone belts: the Musoma-Mara, Kilimafedha, Iramba-Sekenke, Shinyanga-Malita, Nzega and Sukumaland greenstone belts. Although these greenstone belts share some common geological features, differences in age and geochemical signature between the individual greenstone belts indicate that their stratigraphy and geological evolution must be treated separately (e.g. Manya et al., 2007; Manya and Maboko, 2008).

The Sukumaland Greenstone Belt comprises a series of individual greenstone fragments separated by shear zones and granitoid intrusions. These fragments appear to share common stratigraphic features (e.g. Borg et al., 1990; Borg, 1994) similar to the Nyanzian and Kavirondian Supergroups (Manya and Maboko, 2003), but each fragment is large enough to be defined as a greenstone belt in its own right (Cook et al., 2015). The Nyanzian

Supergroup in the Sukumaland Greenstone Belt was subdivided into Lower and Upper Nyanzian (Manya and Maboko, 2003). The Lower Nyanzian is dominated by tholeiitic mafic volcanics with minor felsic volcanics and shale. Sm-Nd whole rock model ages (e.g. Manya and Maboko, 2003; Manya and Maboko, 2008; Cook et al., 2015) indicate that the mafic volcanics of the Lower Nyanzian in the Sukumaland Greenstone Belt were erupted at ca. 2820 Ma. Based on their similar eruption ages, geochemistry and Nd isotopic signature the mafic volcanics of the lower Nyanzian have been grouped into the Kiziba Formation (Cook et al., 2015) that was interpreted to have formed in an oceanic plateau-like environment. The Kiziba Formation has been metamorphosed to lower amphibolite facies (Cook et al., 2015). The Lower Nyanzian is overlain by the Upper Nyanzian, which is composed of shale, volcanoclastics, ironstone, chert, sandstone, siltstone and mudstone (Borg et al., 1990; Borg, 1994). In the Geita Greenstone Belt (GGB, Sanislav et al., 2014), which forms the northern part of the Sukumaland Greenstone Belt (Fig. 1), the contact between the mafic volcanics of the Kiziba Formation and the Upper Nyanzian is marked by a major shear zone (Cook et al., 2015). The entire sequence is complexly deformed with eight deformation events identified in the Upper Nyanzian sequence that hosts the Nyankanga, Geita Hill and Matandani-Kukuluma gold deposits in the GGB (Sanislav et al., 2015, 2017; Figs 1, 2). The Kavirondian Supergroup (Manya and Maboko, 2003) occurs as isolated outcrops that unconformably overly the Upper Nyanzian and is composed of conglomerate, grit, quartzite and sandstone (e.g. Borg et al., 1990; Borg, 1992, 1994).

The northern part of the GGB is intruded by 2620-2660 Ma (Sanislav et al., 2014) high-K granite batholiths while the southern part of the GGB is bordered by gneiss from which it is separated by a ductile shear zone. The eruption of the mafic volcanics forming the Kiziba Formation in the GGB was dated at ~ 2820 Ma (Manya and Maboko, 2008; Cook et al., 2015), whilst the maximum depositional age for the Upper Nyanzian sediments has been

variably given as 2771 (Chamberlain and Tosdal., 2007) and 2702 Ma (Sanislav et al., 2014). Borg and Krogh (1999) dated a diorite sill (Sanislav et al., 2015) that intruded the ironstones in the Geita Hill deposit at 2699±9 Ma confirming that the sedimentation of the Upper Nyanzian in the Geita Greenstone Belt probably ceased by ~ 2700 Ma. Detailed mapping (Sanislav et al., 2015, 2016) around the Nyankanga and Geita Hill gold deposits indicate that the Upper Nyanzian sediments experienced an early extensional shearing event (D_1) followed by four compressional folding events (D_2-D_5) and three transpressional to transtensional brittle-ductile shearing events along discrete shear zones (D_6-D_8). Zircon ages from intrusive porphyries within the greenstone belt and the surrounding granite constrain all tectonic activity between 2820 and 2620 Ma (Manya and Maboko, 2008; Sanislav et al., 2014).

Petrographic description of the Kukuluma Intrusive Complex

The Kukuluma Intrusive Complex (KIC) consists of a series of NW trending intermediate igneous rocks (Fig. 2) that intruded the folded sequence of the Upper Nyanzian sediments, during the D_2-D_3 compressional stages affecting the GGB, sometime between 2680-2700 Ma (Kwelwa, 2017). Three major gold deposits, Matandani, Kukuluma and Area 3 W, occur along the contact between the KIC and the sediments (Fig. 2). The KIC is dominated by equigranular, fine- to medium-grained and locally porphyritic, intermediate intrusives (Fig. 3) and subordinate felsic (Fig. 3) porphyritic dykes.

The intermediate intrusive bodies are weakly to moderately foliated, indicating syn-D_3 emplacement (using the deformation scheme of Sanislav et al., 2015). The mineralogy is dominated by plagioclase (30-45 %), amphibole (30-40 %), alkali-feldspar (5-25 %), biotite (5-15%) pyroxene (5-10%) and quartz (5-20%). Based on the mineralogical composition the intermediate intrusives of the KIC can be separated into a diorite suite (gabbro-diorite and diorite; Figs. 3a and b) and a monzonite suite (monzodiorite and monzonite; Figs. 3c and d).

The feldspars are only partly sericitized (Figs. 3b and d) while some of the mafic minerals are partly replaced by metamorphic actinolite. Accessory minerals include apatite, magnetite, and rutile. Minor chlorite and carbonate are present as disseminated minerals, partly replacing the mafic minerals or along veins.

The felsic porphyritic dykes (Figs. 3e and f) show a narrower variation in their mineralogical composition. Their mineralogy is dominated by quartz (15-40 %), plagioclase (50-70%), K-feldspar (5-40%), biotite (5-15%) and amphibole (1-10%). The main accessory minerals are apatite and zircon. Based on their mineralogical composition the felsic phase of the KIC varies between granodiorite and tonalite. The plagioclase is partly sericitized and the mafic minerals are partly replaced by chlorite.

Methodology for major and trace element analyses

Whole rock geochemical analyses were performed at the Advanced Analytical Centre at James Cook University (JCU) on samples collected from drill core. All samples were collected away from the mineralized zones to minimize the effect of alteration. All samples were studied under the petrographic microscope and only samples that showed the minimum alteration were selected for further analyses. Approximately 1 kg of material was milled from each sample to a fine powder in a tungsten carbide ring mill. Major elements were analysed by conventional X-ray fluorescence (XRF) using a Bruker-AXS S4 Pioneer XRF Spectrometer on fused beads. The fused beads were prepared from rock powders mixed with 12:22 borate flux (XRF Scientific Limited, Perth, Australia) at 1:8 sample to flux ratio that were fused to glass after heating to 1050 °C in a F-M 4 Fusion Bead Casting Machine (Willunga, Australia). Chips of the fused beads were mounted into a standard epoxy puck and analysed for a range of trace elements using a Geolas Pro 193 nm ArF Excimer laser ablation unit (Coherent) coupled to a Varian 820 quadrupole ICP-MS. Helium was used as the carrier

gas (0.8 l/min), which was subsequently mixed with Ar via a mixing bulb between the ablation cell and the ICP-MS to smooth the ablation signal. Laser energy density was set to 6 J/cm^2, and the laser spot size and repetition rate were set to 120 µm and 10 Hz, respectively. Each fused bead was analysed 3 times and average values are reported. The ICP-MS was tuned to ensure robust plasma conditions and low oxide production levels (≤ 0.5% ThO) with the plasma power set at 1.25 kW. NIST SRM 610 glass was used as a bracketed external standard using the standard reference values of Spandler et al. (2011). Data were quantified using Ca (as previously determined by XRF on the same fused bead) as the internal standard, and data were processed using the Glitter software (Van Achterbergh et al., 2001). To monitor precision and accuracy of the analyses, we analysed Hawaiian basalt reference glass (KL2-glass; n=21) as a secondary standard (Jochum et al., 2006). The precision for REE analyses by LA-ICP-MS is better than 5% (mostly <3%), and the accuracy is often <2%. The standard reference material NIST612 (n=11) was analysed as a ternary standard. The precision for all the elements, besides Zn (3.5%) and Ge (~8.3%,) is <2%, and <1% for REE. The accuracy for all the elements (standard reference concentrations taken from Spandler et al., 2011) is <3%. The only exceptions are Tb (6.5%), Ge (~8.3%), Sb (~9%), and Zn (~5.3%) where relatively large uncertainties in the NIST612 glass have to be taken into consideration.

Alteration and element mobility

The KIC rocks are deformed, metamorphosed and locally overprinted by hydrothermal alteration related to gold mineralisation concentrated along its margins. The top 100 meters of the intrusive complex is highly weathered so that all samples were collected from diamond drill holes that intercepted the intrusive complex at more than 400 meters below the surface, and away from mineralised zones. Petrographic examination of the samples revealed minor

carbonate and chlorite alteration indicating that the samples have been hydrated and carbonated. The loss of ignition (LOI) values of up to 5.5% confirms the petrographic observations and requires that all samples be screened for element mobility. On the alteration boxplot of Large et al. (2001), which combines the alteration index of Ishikawa ($100(K_2O+MgO)/(K_2O+MgO+Na_2O+CaO)$) and the chlorite-carbonate-pyrite alteration index ($(100(MgO+FeO)/(MgO+FeO+Na_2O+K_2O)$), all samples plot (Fig. 4a) into the field of least altered rocks. However, to further test the element mobility for the KIC samples we used only the monzonite and diorite suites, because the higher number of samples allows compositional variations induced by post-magmatic alteration to be identified more easily. Na, K, Rb and Sr are all easily mobilised during low-temperature hydrothermal alteration and metamorphism. The post-magmatic disturbance of Na, K, Rb and Sr by hydrothermal alteration and metamorphism can be tested by plotting their concentration against the LOI values. A lack of correlation indicates little or no significant disturbance while well-correlated trends indicate significant disturbance and mobility (e.g. Papoulis et al., 2004; Harvey et al., 2014). The lack of any correlation between these elements and the LOI values (Fig. 4b, c, d and e) combined with their coherent behaviour on other geochemical plots suggests that the post-magmatic alteration did not significantly mobilise these elements, and they can, therefore, be used for petrogenetic interpretations. In general REE and HFSE are considered immobile during hydrothermal alteration and greenschist facies metamorphism, but situations where the REE were mobile have been documented (e.g. Wood et al., 1976; Condie et al., 1977); with the LREE considered to be more mobile than the HREE (Sun and Nesbit, 1978). To test the mobility of the REE from the KIC rocks, we plotted the concentration of La against Zr (Fig. 4f), and to test the mobility of the HFSE we plotted the concentration of Nb against Zr (Fig. 4g). The strong positive correlation that exists between these elements in combination with the coherent behaviour of the REE and HFSE on

chondrite and primitive mantle normalised plots indicate that these elements most probably retained their original concentrations. The ratio of highly incompatible elements such as Th and U should be near chondritic ($Th/U_{chondrite}$= 3.63; Sun and McDonough, 1989) unless disturbed by alteration processes when U is mobile under oxidizing conditions. The average Th/U ratio of all KIC rocks ($Th/U_{monzonite}$=3.65; $Th/U_{diorite}$= 2.92; $Th/U_{granodiorite}$= 2.92) is near chondritic suggesting little to no mobility of these elements during hydrothermal alteration and metamorphism.

The geochemistry of the KIC

The geochemical composition of the KIC (Table 1 and Fig. 5) is characterised by: intermediate SiO_2 (59.17 wt%), moderate #mg (0.47), high Al_2O_3 and FeO (15.83 wt% and 5.66 wt% respectively) and moderate MgO (2.78 wt%). The K_2O/Na_2O ratio is less than 1 (0.70) and $CaO+Na_2O$ is more than 8 (8.82%). The Y content is low (14.5 ppm) and Sr is high (765 ppm) with an average Sr/Y ratio of 59. The HREE are depleted relative to the LREE with an average La/Yb ratio of 42 and the Cr content is moderately high (62 ppm). The chondrite normalized REE pattern (Fig. 6) show fractionated patterns while the primitive mantle normalized multi-element patterns show negative Nb and Ti anomalies and a general enrichment in the large ion lithophile elements (LILE).

The monzonite suite

The geochemical composition of rocks that belong to the monzonite suite (Fig. 5; Table 1) from the KIC is characterized by intermediate SiO_2 (51.7- 62.1 wt%), FeO (3-9 wt%), MgO (2.5-5.6wt%) and CaO (3.8-7 wt%), moderate K_2O (0.9-3.6 wt%), high Al_2O_3 (14.4-16.5 wt%) and Na_2O (4.5-6.6 wt%) and low TiO_2 (0.4-0.6 wt%). They have high $CaO+Na_2O$ (8.6-12.9), high Sr (537-1563 ppm) and high LREE (La_n = 241-777 ppm; the subscript "n" refers to chondrite normalized). These features combined with a low K_2O/Na_2O

ratio (0.1-0.8), low Y (11-30 ppm), low HREE (Yb_n = 4-11) and high Sr/Y and La/Yb ratios (30-119 and 67-102 respectively) indicate that the monzonite suite has geochemical characteristics similar to adakites, sanukitoids and Closepet-type granite. Martin et al (2005) suggested that less differentiated sanukitoids (SiO_2<62 wt%) are similar to LSA and Closepet-type granite. However, rocks that belong to the monzonite suite from the KIC have, on average, higher Y, Yb and La/Yb than the LSA, higher #mg, Sr, Cr, Sr/Y and La/Yb than the Closepet-type granite, and higher La/Yb than the average sanukitoid. At the same time the monzonite suite has lower TiO_2, #mg, Sr, Cr, Ni and Sr/Y than the LSA, lower TiO_2, Y, Yb than the Closepet-type granite and lower Cr compared to the average sanukitoid. The chondrite normalized REE pattern (Fig. 6a) of monzonite suite rocks is subparallel to the pattern from average LSA, sanukitoid and Closepet-type granite and shows the strong LREE enrichment characteristic for these type of rocks. When plotted on a primitive mantle normalized multielement diagram (Fig. 6b) the monzonite suite shows strong negative anomalies for Nb and Ti, and moderate negative anomalies for Zr and Sr. Their pattern is subparallel to that of the LSA, sanukitoids and Closepet-type granite. Notable differences are the positive Sr anomaly for the LSA, the lack of a Sr anomaly in sanukitoids and the lack of a negative Zr anomaly in LSA, sanukitoids and Closepet-type granite.

The diorite suite

Rocks that belong to the diorite suite (Fig. 5; Table 1) have similar SiO_2 (53-63 wt%) contents compared to monzonite suite rocks, but slightly higher Al_2O3 (14.4-17.1 wt%), FeO (2.8-7.8 wt%), and TiO_2 (0.3-0.7 wt%), and slightly lower Na_2O (3.1-5.6 wt%), K_2O (1.2-3.2 wt%) and P_2O_5 (0.1-0.3 wt%). These values combined with K_2O/Na_2O ~ 0.54, $CaO+Na_2O$ ~ 8, low Y (8-12 ppm), low HREE (Yb_n = 3-7 ppm) and high Sr (572-1062 ppm), Cr (49-99 ppm) and LREE (La_n= 45-161 ppm) suggest that the diorite suite also shares geochemical features with sanukitoid, adakite and Closepet-type granite. The average composition of

292 rocks from the diorite suite is similar to the average composition of HSA except for lower
293 SiO_2 (58.6 vs 64.8), higher FeO (6.39 vs. 4.27), higher Cr (75 vs 41) and higher Sr/Y (85 vs
294 56). The chondrite normalized REE pattern (Fig. 6c) is similar to the average HSA and
295 subparallel to, but at lower concentrations than the average LSA, sanukitoid and Closepet-
296 type granite. On a primitive mantle normalized multi-element diagram (Fig. 6d) diorite suite
297 rocks show pronounced negative Nb anomalies, moderately negative Ti anomalies and
298 moderately positive Sr anomalies, all of which are also typical for LSA. The overall pattern is
299 similar to that of HSA, except for the positive Sr anomaly, and is subparallel to the average
300 pattern of LSA, sanukitoid and Closepet-type granite, but at lower concentrations.

301 ## The granodiorite suite

302 Four samples from the KIC were classified as granodiorites. Although the samples
303 were collected a few hundred meters apart their major and trace element composition is
304 almost identical (Fig. 5; Table 1). They have moderate SiO_2 (av. 62.5 wt%), low FeO (av. 4.9
305 wt%), MgO (av. 1.9 wt%), CaO (av. 3.7 wt%) and high K_2O (av. 3.67 wt%) when compared
306 to rocks from the monzonite and the diorite suite. Their K_2O/Na_2O ratio is high (av. 1.1),
307 $CaO+Na_2O$ is low (av. 7.4), Y is low (16 ppm), HREE are low (Yb_n = 10), LREE are
308 moderately high (La_n= 100 ppm), and Sr and Cr content are relatively high (332 and 21 ppm
309 respectively). The lower Sr content (< 400 ppm), a Sr/Y ratio of less than 40 and a La/Yb
310 ratio of less than 20 suggest that the granodiorites cannot be considered to have an adakite-
311 like signature sensu Defant and Drummont (1990). However, as pointed out by Moyen
312 (2009), HSA can have a Sr/Y ratio as low as 20. On a chondrite normalized REE diagram
313 (Fig. 6e) the granodiorites display a subparallel trend to that of the HSA but they plot at
314 higher concentrations. They also show a weak negative Eu anomaly indicative of plagioclase
315 fractionation. On a primitive mantle normalized multi-element diagram (Fig. 6f) their pattern

316 is similar to that of the HSA, except that they have a weak negative Sr anomaly while the
317 HSA have a weak positive Sr anomaly.

318 Petrogenesis of the KIC

319 Relative timing of emplacement

320 Rocks of the granodiorite suite have been dated at 2651 Ma to 2667 Ma (Kwelwa,
321 2017), but there are no direct age data available for rocks forming the monzonite and diorite
322 suites. However, field relationships help constrain their relative timing of emplacement. The
323 intrusives of the monzonite and diorite suites occur as a series of intrusive bodies subparallel
324 to the NW-SE trending regional fabric (Fig. 2). The rocks contain a weakly to well-developed
325 foliation that is subparallel to the axial planar surface of regional D_3 folds (Sanislav et al.,
326 2015, 2017) indicating coeval and syntectonic emplacement. The granodiorite suite rocks are
327 not foliated indicating that their emplacement postdates the emplacement of the diorite and
328 the monzonite suite. Felsic dykes similar in composition to the granodiorite suite outcrop in
329 the Kukuluma and Matandani deposits where they crosscut the folded sequence and are
330 crosscut by brittle ductile shear zones.

331 In the Nyankanga and Geita Hill areas, monzonite and diorite dykes and sills intrude
332 during D_2 and D_3, i.e. at a time relative to deformation that is near identical to the relative
333 timing observed in Kukuluma (Sanislav et al., 2015, 2017). Borg and Krogh (1999) provide
334 an age of 2699±9 Ma for a diorite dyke from Geita Hill, and Chamberlain and Tosdal (2007)
335 report an age of 2698±14 Ma for diorite in the Nyankanga pit where it has been cross cut by
336 several generations of felsic dykes dated at 2685-2696 Ma (Chamberlain and Tosdal, 2007).
337 Therefore, by comparison, the monzonite and diorite suites of the KIC are interpreted to have
338 been emplaced between 2685-2700 Ma.

Depth and source of melts

Fractionated REE patterns (Fig. 6), high Sr/Y and La/Yb ratios (Figs. 7a and b), and low Y and Yb contents suggest that garnet was present as a fractionating or residual phase in the melt (e.g. Martin et al., 2005; Moyen, 2009; Castillo, 2012). However, high Sr/Y and La/Yb ratios can also reflect an enriched source (Moyen, 2009), can be produced by the fractionation of amphibole, and by the delayed crystallization of plagioclase in hydrous mafic magmas (Castillo, 2012), while fractionated REE patterns may result from amphibole fractionation (e.g. Romick et al., 1992; Richards and Kerrich 2007). Continental crust has high Sr/Y and La/Yb ratios, therefore, melting of continental crust and/or mixing with continental crust may impart high Sr/Y and La/Yb to their derivative melts. The low SiO_2 and moderate Mg# of the KIC rocks suggest a mafic to ultramafic source, and preclude any significant contribution from felsic rocks. In mafic melts fractionation of amphibole may increase the La/Yb ratio of the residual melt, but the REE pattern will not develop a strongly concave shape. As magma becomes more dacitic the hornblende REE distribution coefficients increase and magmas develop concave REE patterns and high La/Yb ratios (Romick et al., 1992). So the net effect of amphibole and plagioclase fractionation is an increase in La/Yb and decrease in Dy/Yb (Moyen, 2009), whereas garnet fractionation or partial melting with residual garnet will increase the Dy/Yb ratio in the melt (e.g. Macpherson et al., 2006; Davidson et al., 2007). Kelemen et al. (2003) proposed that melts with a clear garnet (eclogite) signature should have Dy/Yb_n ratios ≥ 1.5. All samples of the monzonite suite and the majority of the diorite suite samples have $Dy/Yb_n > 1.5$ (Fig. 7c) suggesting that their high Sr/Y and La/Yb ratios are related to deep melting. Eclogite melts reacting with the mantle (Kelemen et al., 2003) would decrease both the Dy/Yb and the La/Yb ratios (Fig. 7d) of the initial melt. Therefore, a lack of eclogite melting signature in some of the samples (i.e. the granodiorite suite) does not automatically rule out their

derivation from eclogite/garnet-bearing melts. Moreover, plagioclase crystallization can decrease Sr/Y ratios and increase Y concentrations. Thus, a deep melting signature (based on this ratio) can be erased by large degrees of plagioclase fractionation (e.g. Richard and Kerrich, 2007).

The major element variation diagrams show that for the same SiO_2 content (Fig. 5), the diorite and the monzonite suites display subparallel trends for most of the elements. It is particularly obvious for Al_2O_3, FeO_t, Na_2O, TiO_2 and P_2O_5. Assuming that the two suites were derived from rocks having a similar composition this subparallel evolution of the major elements cannot be explained by magma mixing or by fractional crystallization alone and requires melting at different pressures. For example, the Al_2O_3 content of melts becomes depleted with increasing pressure at the same degree of partial melting (e.g. Hirose and Kushiro, 1993; Spandler et al., 2008). The negative correlation between SiO_2 and Al_2O_3 (Fig. 5a) in the diorite suite may indicate garnet fractionation or residual garnet, which will effectively reduce Al_2O_3 with increasing SiO_2 in the melt (Macpherson et al., 2006; Davidson et al., 2007). The positive correlation observed in the monzonite suite may indicate that garnet was partly consumed during melting. The monzonite suite rocks tend to have higher Na_2O at the same CaO (Fig. 8a) compared to the diorite suite rocks. This can also indicate a higher pressure during melting as Na_2O becomes more compatible in clinopyroxene at higher pressure (e.g. Kogiso et al., 2004).

On chondrite normalized diagrams (Fig. 6) the REE patterns for the two suites are subparallel, but the LREE elements are more fractionated for the monzonite suite than the diorite suite. This is also illustrated by much higher La/Yb_n and Dy/Yb_n ratios (Fig. 7) suggesting that rocks belonging to the monzonite suite may represent deeper melts compared to rocks from the diorite suite. Their primitive mantle normalized trace element patterns (Fig. 6) are also sub-parallel, with the notable difference that the diorite suite rocks have a positive

Sr anomaly while the monzonite suite rocks have negative Sr and Zr anomalies. The presence of a significant positive Sr anomaly in the diorite suite cannot be explained by melting or crystallization unless plagioclase is involved. The lack of any correlation between the Sr/Sr* and the MgO (Fig. 8b) excludes fractionation. Thus, a plagioclase-rich component is required in the melt source region. Alternatively, interaction of the melt with a plagioclase-rich region (assimilation) will produce a similar effect. However, assimilation will result in a large decrease in FeO_t and a large increase in Al_2O_3 with decreasing MgO (e.g. Peterson et al., 2014), which is not the case here. Therefore assimilation can be excluded.

The only viable explanation is that the positive Sr anomaly is related to the source rock. We propose that the diorite suite was formed by melting of garnet-bearing amphibolite and plagioclase was completely transferred into the melt, leaving behind a Sr-depleted (relative to Ce and Nd) residue of garnet-clinopyroxene-rutile eclogite. Further melting of the eclogite with residual rutile produced the monzonite suite with negative Sr and Zr anomalies. Zr and Hf have similar chemical properties and should not fractionate from each other in geological processes; i.e. their ratio should be chondritic in all earth materials (e.g. Zr/Hf=~36.3; Sun and McDounough, 1989). The diorite suite has an average Zr/Hf ratio of 36.8 (Fig. 8c), which is similar to the chondritic value, but the monzonite suite has an average Zr/Hf ratio of 42.7 (Fig. 8c), which exceeds the chondritic value suggesting that these elements were fractionated from each other. Experimental data on amphibole/melt partition coefficients (e.g. Foley et al., 2002; Tiepolo et al., 2007) have shown that amphibole can fractionate most HFSE causing negative Ti and Nb anomalies, but only high-Mg amphibole can fractionate Zr from Hf. The ability of garnet to fractionate Zr from Hf is dependent on pressure and MgO content (e.g. Green et al., 2000; van Westrenen et al., 1999). The only mineral able to effectively fractionate HFSE from each other is rutile (Stalder et al., 1998; Foley et al., 2000). If rutile was the residual phase, the Nb/La and Zr/Sm ratios of the melt

414 will correlate positively (Münker et al., 2004), but if high-Mg amphibole was the residual
415 phase the melt ratios of these elements will correlate negatively. The monzonite suite shows a
416 clear positive correlation between Nb/La and Zr/Sm (Fig. 8d) implying residual rutile.
417 However, the diorite suite shows no correlation between these two ratios. Rutile cannot
418 coexist with basaltic melts arising from the partial melting of peridotite (e.g. Ryerson and
419 Watson, 1987; Woodhead et al., 1993; Thirlwall et al., 1994), because it reacts with the
420 olivine to form orthopyroxene and ilmenite. Thus, the most likely source for the monzonite
421 suite is rutile-bearing, garnet-clinopyroxene eclogite.

422 ## Melt mantle interaction

423 The low SiO_2 content, average Mg numbers, and relatively high Ni and Cr
424 concentrations indicate that the source rocks for the KIC must be mafic or ultramafic. Their
425 intermediate composition ($SiO_2 \leq 62$ wt%) suggests that fractionation played a minor role in
426 their petrogenesis and they are close to primary magmas. From this point of view the rocks of
427 the KIC resemble LSA and sanukitoid. However, there are some important differences.
428 Firstly, at the same SiO_2 content the rocks of the KIC have much lower MgO compared to
429 LSA (Fig. 5b). Secondly, the rocks of the KIC overlap the field of mafic experimental melts
430 (Figs 3a,b and f), whereas LSA rocks plot above it, and the sanukitoids overlap with it, but
431 only for low MgO concentrations. Because of their low SiO_2, high Mg numbers and high Cr
432 and Ni concentrations, the LSA and the sanukitoids are commonly interpreted to have formed
433 by partial melting of mantle peridotite metasomatised by felsic melts (e.g. Shirey and
434 Hanson, 1984; Rapp et al., 1999; Martin et al., 2005). The rocks of the KIC have lower Mg
435 numbers (at the same SiO_2 content; Fig. 5b) and much lower Cr, Ni, Sr, K, Rb and Nb
436 concentrations compared to LSA rocks and the sanukitoids (Fig. 9 and Table 1). The
437 difference between KIC rocks and LSA rocks is clearly illustrated in Figure 9 where the

composition of KIC rocks overlaps the composition of the HSA, and closely resembles the composition of experimental melts of basalt (Figs. 7a and b).

On the K vs Rb diagram (Fig. 9a) some of the LSA rocks plot subparallel to the Y-axis suggesting high K/Rb ratios, which were interpreted to reflect Rb depletion by selective melting of metasomatic amphibole in a peridotite source (e.g. Martin et a., 2005 and references therein). However, in the absence of metasomatism, both peridotite and basaltic melts result in K/Rb ratios much lower than average oceanic basalt (K/Rb=1071; Sun and McDonough, 1989). High Sr contents can reflect deep melting at pressures above the plagioclase stability field, melting of a source that was already high in Sr, and/or melt interaction with high-Sr geological materials (e.g. Moyen, 2009). Given the low SiO_2 ($\leq$ 62 wt%) of the KIC samples, their source rock must have been mafic or ultramafic. Experimental melting of basalt produced liquids with up to 1000 ppm Sr (Fig. 9b), but to achieve the high Sr observed in LSA, interaction with mantle peridotite is required (e.g. Martin et al., 2005). Rocks from the diorite and granodiorite suites plot within the fields of basaltic melts and HSA (Fig. 9b), while some of the samples from the monzonite suite plot at higher Sr values (~1500 ppm) within the field of LSA, which may indicate some level of interaction with mantle peridotite. However, if the source of the KIC rocks was mafic lower crust (Sr = 348 ppm; Rudnick and Gao, 2003; Sr = 289 ppm; Hacker et al., 2015) rather than an average oceanic basalt (Sr = 90 ppm; Sun and Mcdonough, 1989), than high Sr values observed in the monzonite suite do not necessarily require interaction with peridotite mantle. Maybe the most useful ratio to use when separating melts derived from partial melting of metasomatised mantle peridotite (LSA) and melts derived by partial melting of mafic rocks (HSA) is the Cr/Ni ratio (Fig. 9c; Martin et al., 2005). The Cr/Ni ratio for KIC samples (Fig. 9c) is clearly distinct from that of the LSA and overlaps the field of the HSA suggesting a mafic source and minimum interaction with the mantle. The lack of correlation between the

Cr/Ni ratio and the Mg# (Fig. 9d) suggests that the Cr/Ni ratio of the KIC samples is a source characteristic and not dependent on fractionation.

Tectonic setting

The rocks of the KIC have major and trace element signatures similar to "adakitic' rocks. Although the original description of adakites (e.g. Defant and Drumkond, 1990) specifically indicates that their geochemical signature is derived from partial melting of a subducted slab, it is clear now that high Sr/Y and La/Yb ratios alone cannot be used to unequivocally indicate a subduction setting (e.g. Moyen, 2009; Castillo, 2012), and rocks with an "adakitic" signature can form in different tectonic settings as well. The KIC was emplaced syn-tectonically along axial planar surfaces of upright regional folds suggesting a period of crustal thickening between 2685-2700 Ma. The age data from the northern half of the Tanzania Craton (e.g. Kabete et al., 2012; Sanislav et al., 2014) suggest that growth of this part of the craton started at ~ 2820 Ma with extensive tholeiitic mafic volcanism (e.g. Manya and Maboko, 2003, 2008; Cook et al., 2015) followed by a period dominated by the intrusion of diorite and TTG and completed with the intrusion of the 2620-2660 Ma high-K granites (Sanislav et al., 2014). Thus, the KIC was emplaced during the transition period from higher depth TTG magmas to shallower depth high-K magmas.

Cook et al. (2015) proposed that the ~ 2820 Ma mafic volcanics (Kiziba Formation) that form the base of the stratigraphic sequence (Lower Nyanzian) in the Sukumaland Greenstone Belt were emplaced in an oceanic plateau like setting. However, it is unclear at the moment whether or not the Upper Nyanzian sediments (intruded by the KIC) were deposited on top of the Kiziba Formation or the two units were tectonically juxtaposed. In the Geita region the contact between the two units is structural (Cook et al., 2015), but there appears to be evidence that the Geita Greenstone Belt is underlain by the mafic rocks of the Kiziba Formation suggesting that crustal growth in this part of Tanzania occurred by partial

melting and maturation of an oceanic plateau by lower crustal delamination/modification (e.g. Vlaar et al., 1994; Zegers and van Keken, 2001; Bedard, 2006; Bedard et al., 2013; Cook et al., 2015). Chiaradia (2015) showed that there is a strong correlation between the Sr/Y ratio and MgO content of recent arc magmatism, and the upper plate thickness indicating that source processes (slab melting, slab melt-mantle interactions) do not play a major role in the generation of high Sr/Y signatures. This implies that high Sr/Y ratios occur at lower MgO content, suggesting that thicker crust favours magma evolution at deeper levels, thus Sr/Y increases steadily with magmatic differentiation (Fig. 10a). In contrast, Archean rocks show a sudden increase of the Sr/Y ratio between ~2.5 and ~0.5 wt% MgO (Fig. 10a) suggesting that, as opposed to modern arc lava, source processes control the Sr/Y ratio of Archean rocks (Chiaradia, 2015). Source processes may include partial melting in the garnet stability field of subducted mafic crust or partial melting of delaminated lower mafic crust.

To investigate a possible subduction component in the generation of the KIC rocks we use Th/U vs Zr/Hf ratios. Partial melting in the mantle wedge can be excluded, as detailed above, based on the presence of Nb and Ti depletion due to residual rutile, which cannot coexist with basaltic melts arising from the partial melting of peridotite (e.g. Ryerson and Watson, 1987; Woodhead et al., 1993; Thirlwall et al., 1994) because it reacts with the olivine to form orthopyroxene and ilmenite. Given the highly incompatible behaviour of Th and U, normal magmatic processes cannot significantly fractionate these elements from each other. U and Th are easily fractionated during surface processes, because of the higher mobility of U during weathering and under oxidizing conditions. Seafloor alteration and addition of slab fluids will lower the Th/U ratio while dehydration and addition of sediment melts will increase the Th/U ratio (e.g. Bebout, 2007). Figure 10b shows that the diorite and the granodiorite suites have almost MORB-like Th/U and Zr/Hf ratios, thus precluding a

513 subduction component. The monzonite suite has higher Zr/Hf ratios due to residual rutile (see
514 above), and the Th/U ratio varies between the values for the lower mafic crust end-member of
515 Hacker et al. (2015) and the values for the average lower continental crust of Rudnick and
516 Gao (2003). Overall, the KIC shows a very narrow variation in Th/U ratios, which is more
517 consistent with partial melting of the mafic lower crust than partial melting of a subducted
518 oceanic crust.

519

520 Conclusions

521 In general Archean igneous rocks with adakite-like signature are interpreted to
522 indicate a subduction setting. We have shown that although the rocks of the KIC can be
523 easily classified as "adakites", detail screening of their composition revealed important
524 differences. Given the recognition that rocks with adakite-like signature can form in a variety
525 of tectonic settings from non-unique petrogenetic processes requires a re-examination of the
526 existing Archean datasets. Higher Archean geothermal gradients would have favoured the
527 development of thicker lithospheric roots and partial to complete eclogitization of the mafic
528 lower crust; the removal of the eclogitised crust by delamination would favour partial melting
529 of the thickened lower crust to generate adakite-like rocks. This scenario is similar to the
530 interpretation of the post-tectonic adakite-like rocks from the Tibetan Plateau with the main
531 difference that the KIC is syn-tectonic. Alternatively, the KIC formed by partial melting of
532 eclogitised mafic lower crust of an Archean oceanic plateau.

533 Acknowledgments

534 This study is part of a PhD study undertaken by the first author at James Cook University.
535 SDK would like to thank James Cook University for waiving the tuition fees and Geita Gold

Mine for providing the research funding for this study. Craig Duvel, Hatari Mjinja and the exploration team from Geita Gold Mine are greatly acknowledged for all of their support during this project. Carl Spandler is acknowledged for reading an early version of the manuscript and providing some thoughtful comments. Detailed comments by two anonymous reviewers are greatly acknowledged for helping improve the quality of the manuscript.

References

Atherton, M.P., Petford, N., 1993. Generation of sodium-rich magmas from newly underplated basaltic crust. Nature 362, 144-146.

Bebout, G.E., 2007. Metamorphic chemical geodynamics of subduction zones. Earth and Planetary Science Letters 260, 373-393.

Bedard, J.H., 2006. A catalytic delamination-driven model for coupled genesis of Archaean crust and sub-continental lithospheric mantle. Geochimica et Cosmochimica Acta 70, 1188-1214.

Bédard, J.H., Harris, L.B., and Thurston, P.C., 2013. The hunting of the snArc: Precambrian Research, 229, 20-48.

Borg, G., 1992. New aspects on the lithostratigraphy and evolution of the Siga Hills, an Archean granite–greenstone terrain in NW-Tanzania. Z. Angew. Geol. 38, 89–93

Borg, G., 1994. The Geita gold deposit in NW Tanzania. Geology, ore petrography geochemistry and timing events. Geol. Jb. D 100, 545–595.

Borg, G., Lyatuu, D.R., Rammlmair, D., 1990. Genetic aspects of the Geita and Jubilee reef, Archean BIF-hosted gold deposits, Tanzania. Geol. Rundsch. 79, 355–371.

557 Borg, G., Shackleton, R.M., 1997. The Tanzania and NE-Zaire Cratons. In: de Wit, M.J.,
558 Ashwal, L.D. (Eds.), Greenstone Belts. Oxford University Press, Oxford, pp. 608–619.

559 Borg. G., and Krogh, T., 1999. Isotopic age data of single zircons from the Archaean
560 Sukumaland Greenstone Belt, Tanzania. Journal of African Earth Sciences 29, 301-
561 312.

562 Castillo, P. R., 2012. Adakite petrogenesis. Lithos 134-135, 304-316.

563 Chamberlain, C.M., Tosdal, R.M., 2007. U–Pb geochronology of the Lake Victoria
564 Greenstone Terrane, Tanzania. Mineral Deposit Research Unit The University of
565 British Columbia (Research Program on World-class Gold Deposits and Advanced
566 Exploration Projects Owned and/or Joint Ventured to Barrick Gold, Placer Dome,
567 Anglo - Gold Ashanti, Resolute Mining NL as Main Sponsors.

568 Chiaradia, M., 2015. Crustal thickness control on Sr/Y signatures of recent arc magmas: an
569 Earth scale perspective. Scientific Reports 5, 8115.

570 Condie, K.C., 2005. TTGs and adakites: are they both slab melts? Lithos 80, 33–44.

571 Condie, K.C., 2014. Growth of continental crust: a balance between preservation and
572 recycling. Mineral. Mag. 78, 623–637.

573 Condie, K.C., Viljoen, M.J., and Kable, E.D.J., 1977. Effects of alteration on element
574 distributions in Archaean tholeiites from the Barberton greenstone belt, South Africa.
575 Contributions to Mineralogy and Petrology 64, 75-89.

576 Cook, Y.A., Sanislav, I.V., Hammerli, J., Blenkinsop, T.G., and Dirks, P.H.G., 2015. A
577 primitive mantle source for the Neoarchean mafic rocks from the Tanzania
578 Craton. Geoscience Frontiers-in press.

579 Davidson, J., Turner, S., Handley, H., Macpherson, C., Dosseto, A., 2007. Amphibole
580 "sponge" in arc crust? Geology 35, 787–790.

581 Defant, M.J., Drummond, M.S., 1990. Derivation of some modern arc magmas by melting of
582 young subducted lithosphere. Nature 347, 662–665.

583 Drummond, M.S., Defant, M.J., 1990. A model for trondhjemite–tonalite–dacite genesis and
584 crustal growth via slab melting: Archaean to modern comparisons. Journal of
585 Geophysical Research 95, 21503-21521.

586 Foley, S., Tiepolo, M., Vannucci, R., 2002. Growth of early continental crust controlled by
587 melting of amphibolite in subduction zones. Nature 417, 837– 840.

588 Foley, S.F., Barth, M.G., Jenner, G.A., 2000. Rutile/melt partition coefficients for trace
589 elements and an assessment of the influence of rutile on the trace element
590 characteristics of subduction zone magmas. Geochim. Cosmochim. Acta 64, 933–938.

591 Gabert, G., 1990. Lithostratigraphic and tectonic setting of gold mineralization in the
592 Archaean Cratons of Tanzania and Uganda, East Africa. Precambrian Research 46,
593 59–69.

594 Gao, S., Rudnick, R.L., Yuan, H.L., Liu, X.M., Liu, Y.S., Xu, W.L., Lin, W.L., Ayerss, J.,
595 Wang, X.C., Wang, Q.H., 2004. Recycling lower continental crust in the North China
596 craton. Nature 432, 892–897.

597 Goss, A.R., Kay, S.M., Mpodozis, C., 2011. The geochemistry of a dying continental arc: the
598 Incapillo Caldera and Dome Complex of the southernmost Central Andean Volcanic
599 Zone (28°S). Contributions to Mineralogy and Petrology 161, 101-128.

600 Green, T.H., Blundy, J.D., Adam, J., Yaxley, G.M., 2000. SIMS determination of trace
601 element partition coefficients between garnet, clinopyroxene and hydrous basaltic
602 liquids at 2 – 7.5 GPa and 1080–1200 °C. Lithos 53, 165– 187.

603 Hacker, B.R., Kelemen, P.B., Behn, M.D., 2015. Continental lower crust. Annual Review of
604 Earth and Planetary Sciences 43, 167–205.

605 Harpum, J.R., 1970. Summary of the geology of Tanzania: structure and geotectonics of the
606 Precambrian. Tanzania Geol. Surv. Mem. 1 Part V, 58 pp.

607 Harvey, J, Savov, IP, Agostini, S., Cliff, R.A., and Walshaw, R., 2014. Si-metasomatism in
608 serpentinized peridotite: the effects of talc-alteration on strontium and boron isotopes
609 in abyssal peridotites from Hole 1268a, ODP Leg 209. Geochimica et Cosmochimica
610 Acta, 126, 30–48.

611 Hirose K, Kushiro I. 1993. Partial melting of dry peridotites at high pressures: determination
612 of compositions of melts segregated from peridotite using aggregates of diamond.
613 Earth Planet. Sci. Lett. 114:477–89.

614 Jayananda, M., Martin, H., Peucat, J.-J. and Mahabaleswar, B., 1995. Late Archaean crust-
615 mantle interactions in the Closepet granite, Southern India: evidence from Sr–Nd
616 isotopes, major and trace element geochemistry. Contributions to Mineralogy and
617 Petrology **119**, 314–29.

618 Jochum, K.P., Stoll, B., Herwig, K., et al., 2006. MPI-DING reference glasses for in situ mi-
619 croanalysis: new reference values for element concentrations and isotope ratios.
620 Geochemistry, Geophysics, Geosystems 7, http://dx.doi.org/10.1029/2005GC001060.

621 Kabete, J.M., Groves, D.I., McNaughton, N.J., Mruma, A.H., 2012a. A new tectonic and
622 temporal framework for the Tanzanian Shield: implications for gold metallogeny and
623 undiscovered endowment. Ore Geology Reviews 48, 88–124.

624 Kabete, J.M., McNaughton, N.J., Groves, D.I., and Mruma, A.H., 2012b. Reconnaissance
625 SHRIMP U–Pb zircon geochronology of the Tanzania Craton: Evidence for
626 Neoarchean granitoid–greenstone belts in the Central Tanzania Region and the
627 Southern East African Orogen. Precambrian Research 216– 219, 232– 266.

628 Kamber, B.S., Ewart, A., Collerson, K.D., Bruce, M.C., McDonald, G.D., 2002. Fluid-mobile
629 trace element constraints on the role of slab melting and implications for Archean
630 crustal growth models. Contributions to Mineralogy and Petrology 144, 38–56

631 Kay, R.W., 1978. Aleutian magnesian andesites: melts from subducted Pacific Ocean crust.
632 Journal of Volcanology and Geothermal Research 4, 117–132.

633 Kelemen, P.B., K. Hanghøj, and A.R. Greene 2003. One view of the geochemistry of
634 subduction-related magmatic arcs with an emphasis on primitive andesite and lower
635 crust, in The Crust, (R.L. Rudnick, ed.), Vol. 3, Treatise on Geochemistry, (H.D.
636 Holland and K.K. Turekian, eds.), Elsevier-Pergamon, Oxford, 593-659,

637 Kogiso T., Hirschmann M.M., Petermann M., 2004. High-pressure partial melting of mafic
638 lithologies in the mantle. Journal of Petrology 45, 2407-2422.

639 Kwelwa, S., 2017. Geological controls on gold mineralization in the Kukuluma Terrain,
640 Geita Greenstone Belt, NW Tanzania. PhD Thesis, James Cook University,
641 Townsville, 205pp.

642 Kwelwa, S., Manya, S., Vos, I.M.A., 2013. Geochemistry and petrogenesis of intrusions of
643 the Golden Pride gold deposit in the Nzega Greenstone Belt, Tanzania. African
644 Journal of Earth Sciences, 86, 53-64.

645 Large, R.R., Gemmell, J.B., Paulick, H., and Huston, D.L., 2001. The alteration box plot—A
646 simple approach to understanding the relationship between alteration mineralogy and
647 lithogeochemistry associated with volcanic-hosted massive sulfide deposits:
648 Economic Geology, 96, 957–971.

649 Macpherson, C.G., Dreher, S.T., Thirwall, M.F., 2006. Adakites without slab melting: high
650 pressure processing of basaltic island arc magma, Mindanao, the Philippines. Earth
651 and Planetary Science Letters 243, 581–593.

652 Manikyamba, C., Kerrich, R., Khanna, T.C., Subba Rao, D.V., 2007. Geochemistry of
653 adakites and rhyolites from the Neoarchaean Gadwal greenstone belt, Eastern
654 Dharwar craton India:implications for sources and geodynamic setting. Canadian
655 Journal of Earth Sciences 44, 1517–1535.

656 Manya, S., and Maboko, A. H. M., 2008. Geochemistry of the Neoarchean mafic volcanic
657 rocks of the Geita area, NW Tanzania: Implications for stratigraphical relationships in
658 the Sukumaland greenstone belt. Journal of African Earth Sciences 52, 152-160.

659 Manya, S., and Maboko, M. A. H., 2003. Dating basaltic volcanism in the Neoarchaean
660 Sukumaland Greenstone Belt of the Tanzania Craton using the Sm–Nd method:
661 implications for the geological evolution of the Tanzania Craton. Precambrian
662 Research 121, 35-45.

663 Manya, S., Maboko, M.A.H., 2008. Geochemistry of the Neoarchean mafic volcanic rocks
664 of the Geita area, NW Tanzania: implications for stratigraphical relationships in the
665 Sukumaland Greenstone belt. J. Afr. Earth Sci. 52, 152–160.

666 Manya, S., Maboko, M.A.H., Nakamura, E., 2007. Geochemistry of high-Mg andesite and
667 associated adakitic rocks in the Musoma-Mara greenstone belt, northern Tanzania:
668 possible evidence for Neoarchaean ridge subduction?''. Precambrian Research 159,
669 241–259.

670 Manya, S.,Maboko,M.A.H., 2003. Dating basaltic volcanism in the Neoarchean Sukumaland
671 Greenstone Belt of the Tanzania Craton using Sm–Nd method: implications for the
672 geological evolution of the Tanzania Craton. Journal of African Earth Sciences 121,
673 35–45.

674 Martin, H., 1999. The adakitic magmas: modern analogues of Archaean granitoids. Lithos 46
675 (3), 411–429.

676 Martin, H., Moyen, J.F., Rapp, R.P., 2010. The sanukitoid series: magmatism at the
677 Archaean-Proterozoic transition. Earth and Environmental Science. Transactions of
678 the Royal Society of Edinburgh 100 (1–2), 15–33.

679 Martin, H., Smithies, R.H., Rapp, R., Moyen, J.F., Champion, D., 2005. An overview of
680 adakite, tonalite–trondhjemite–granodiorite (TTG), and sanukitoid: relationships and
681 some implications for crustal evolution. Lithos 79, 1–24.

682 Mohan, M.R., Piercey, S.J., Kamber, B.S., Sarma, D.S., 2013. Subduction related tectonic
683 evolution of the Neoarchean eastern Dharwar Craton, southern India: new
684 geochemical and isotopic constraints. Precambrian Research 227, 204–226.

685 Moyen, J.-F., 2009. High Sr/Y and La/Yb ratios: The meaning of the "adakitic signature".
686 Lithos 112, 556–574.

687 Moyen, J.-F., 2011. The composite Archaean grey gneisses: petrological significance, and
688 evidence for a non-unique tectonic setting for Archaean crustal growth. Lithos 123,
689 21-36.

690 Moyen, J.-F., Martin, H., 2012. Forty years of TTG research. Lithos 148, 312–336

691 Papoulis D., Tsolis-Katagas, P., and Katagas, C., 2004. Monazite alteration mechanisms and
692 depletion measurements in kaolins. Applied Clay Science, 24, 271–285.

693 Peterson, M. E., A. E. Saal, E. Nakamura, H. Kitagawa, M. D. Kurz, and A. M.
694 Koleszar (2014), Origin of the "ghost plagioclase" signature in Galapagos melt
695 inclusions: New evidence from Pb isotopes. Journal of Petrology, 55, 2193–2216.

696 Polat, A., Kerrich, R., 2001. Magnesian andesites, Nb-enriched basalt–andesites, and adakites
697 from late-Archean 2.7 Ga Wawa greenstone belts, Superior Province, Canada:
698 implications for late Archean subduction zone petrogenetic processes. Contributions
699 to Mineralogy and Petrology 141 (1), 36–52.

700 Quennell, A.M., McKinley, A.C.M., Aiken, W.G., 1956. Summary of the geology of
701 Tanganyika: introduction and stratigraphy. Tanganyika Geol. Surv. Mem. 1 (Pt. 1)
702 264 pp..

703 Rapp, R.P., Shimizu, N., Norman, M.D., Applegate, G.S., 1999. Reaction between slab-
704 derived melts and peridotite in the mantle wedge: experimental constraints at 3.8 GPa.
705 Chemical Geology 160, 335–356.

706 Richards, J. P., and Kerrich, R. 2007. Adakite-like rocks: their diverse origins and
707 questionable role in metallogenesis. Economic Geology 102, 537–576.

708 Rollinson, H., 1997. Eclogite xenoliths in west African kimberlites as residues from Archean
709 granitoid crust formation. Nature 389, 173–176.

710 Romick, J.D., Kay, S.M., Kay, R.M., 1992. The influence of amphibole fractionation on the
711 evolution of calc-alkaline andesite and dacite tephra from the central Aleutians,
712 Alaska. Contributions to Mineralogy and Petrology 112, 101–118.

713 Rooney, T.O., Franceschi, P., Hall, C.M., 2011. Water-saturated magmas in the Panama
714 Canal region: a precursor to adakite-like magma generation? Contributions to
715 Mineralogy and Petrology 161, 373-388.

716 Rudnick RL, Gao S. 2003. Composition of the continental crust. See Holland & Turekian
717 2003, pp. 1–64

718 Rudnick, R.L., 1995. Making continental crust. Nature 378, 573–578.

719 Ryerson F. J. and Watson E. B. (1987) Rutile saturation in magmas: Implications for Ti–Nb–
720 Ta depletion in island-arc basalts. Earth and Planetary Science Letters 86, 225–239.

721 Sanislav, I. V., Brayshaw, M., Kolling, S. L., Dirks, P. H. G. M., Cook, Y. A., Blenkinsop,
722 T., 2016. The structural history and mineralization controls on the world-class Geita
723 Hill gold deposit, Geita Greenstone Belt, Tanzania. Mineralium Deposita – in press.

724 Sanislav, I. V., Wormald, R. J., Dirks, P. H. G. M., Blenkinsop, T. G., Salamba, L., Joseph,
725 D., 2014. Zircon U-Pb ages and Lu-Hf isotope systematics from late-tectonic granites,
726 Geita greenstone belt: implications for crustal growth of the Tanzania craton.
727 Precambrian research 242, 187-204.

728 Sanislav, I.V., Kolling, S.L., Brayshaw, M., Cook, Y.A., Dirks, P.H.G.M., Blenkinsop, T.G.,
729 Mturi, M.I., Ruhega, R., 2015. The geology of the giant Nyankanga gold deposit,
730 Geita Greenstone Belt, Tanzania. Ore Geology Reviews 69, 1-16.

731 Shirey, S. B., Hanson, G. N. 1984. Mantle derived Archaean monzodiorites and
732 trachyandesites. Nature 310, 222–4.

733 Shirey, S.B., Hanson, G.N., 1984. Mantle derived Archaean monzodiorites and
734 trachyandesites. Nature 310, 222– 224.

735 Spandler, C., Pettke, T., Rubatto, D., 2011. Internal and external fluid sources for eclogite-
736 facies veins in the Monviso meta-ophiolite, Western Alps: Implications for fluid flow
737 in subduction zones. Journal of Petrology, 52, 1207–1236.

738 Spandler, C., Yaxley, G., Green, D. H. and Rosenthal, A., 2008. Phase relations and melting
739 of anhydrous K-bearing eclogite from 1200 to 1600°C and 3 to 5 GPa. Journal of
740 Petrology 49, 771-795.

741 Stalder, R., Foley, S.F., Brey, G.P. and Horn, I. 1998. Mineral aqueous fluid partitioning of
742 trace elements at 900-1200 degrees C and 3.0-5.7 GPa: New experimental data for
743 garnet, clinopyroxene, and rutile, and implications for mantle
744 metasomatism. Geochimica et Cosmochimica Acta 62, 1781-1801.

745 Stern, R. A. Hanson, G. N. and Shirey S. B.. 1989. Petrogenesis of mantle-derived, LILE-
746 enrichedA rchean monzodiorites and trachyandesites (sanukitoids) in southwestern
747 Superior Province. Canadian Journal of Earth Sciences, 26, 168- 171.

748 Stockley, G.M., 1936. Geology of the south and south-western region of Musoma District.
749 Tanganyika Geol. Surv. Short Pap., 13.

750 Sun, S. -S., McDonough,W. F., 1989. Chemical and isotopic systematics of oceanic basalts:
751 implications for mantle composition and processes. In: Saunders, A.D., Norry, M.J.
752 (Eds.), Magmatism in the Ocean Basins. Geol. Soc. London, London, pp. 313–345.

753 Sun, Shen-SU and Nesbitt, R.W., 1978. Petrogenesis of Archaean ultrabasic and basic
754 volcanics: evidence from the rare earth elements. Contributions to Mineralogy and
755 Petrology 65, 301-325.

756 Tatsumi Y, Ishizaka K. 1981. Existence of andesitic primary magma: An example from
757 Southwest Japan. Earth and Planet Science Letters 53, 124-130.

758 Tatsumi Y. 2006 High-Mg Andesites in the Setouchi Volcanic Belt, Southwestern Japan:
759 Analogy to Archean Magmatism and Continental Crust Formation? Annu Rev Earth
760 Planet Sci, 34, 467—499.

761 Tatsumi, Y., 2008. Making continental crust: the sanukitoid connection. Chinese Science
762 Bulletin 53 (11), 1620–1633.

763 Taylor S. R. and McLennan S. M. 1995 The Geochemical Evolution of the Continental Crust
764 Reviews of Geophysics 22-2, 241-265

765 Thirlwall M. F., Smith T. E., Graham A. M., Theodorou N., HollingsbP., Davidson J. P., and
766 Arculus R. J. (1994) High field strength element anomalies in arc lavas: source or
767 process? Journal of Petrology 35, 819–838.

768 Thorkelson, D.J. and Breitsprecher, K., 2005. Partial melting of slab window margins:
769 genesis of adakitic and non-adakitic magmas. Lithos, 79, 25-41.

770 Tiepolo, M., Oberti, R., Zanetti, A., Vannucci, R., Foley, S., 2007. Trace-element partitioning
771 between amphibole and silicate melt. In: Hawthorne, F.C., Oberti, R., Ventura, G.D.,

Mottana, A. (Eds.), Amphiboles: Crystal Chemistry, Occurrence, and Health Issues: Mineralogical Society of America and Geochemical Society, Reviews in Mineralogy and Geochemistry, 67, pp. 417–452.

Tulloch, A.J., Kimbrough, D.L., 2003. Paired plutonic belts in convergent margins and the development of high Sr/Y magmatism: Peninsular Ranges batholith of Baja-California and Median batholith of New Zealand. Geological Society of America Special Paper 374, 1–21.

van Achterbergh E., Ryan C.G., Jackson S.E., and Griffin, W.L., 2001. Data reduction software for LA-ICP-MS. In: Sylvester P (ed) Laser-ablation-ICPMS in the earth sciences: principles and applications. Mineralogical Association of Canada, Short Course 29, 239–243.

van Westrenen, W., Blundy, J., Wood, B., 1999. Crystal-chemical controls on trace element partitioning between garnet and anhydrous silicate melt. American Mineralogist 84, 838–847.

Vlaar, N.J., van Keken, P.E., and van den Berg, A.P., 1994, Cooling of the Earth in the Archaean: Earth and Planetary Science Letters, v. 121, p. 1–18.

Wang, Q., McDermott, F., Xu, J.F., Bellon, H., Zhu, Y. T., 2005. Cenozoic K-rich adakitic volcanic rocks in the Hohxil area, northern Tibet: lower-crustal melting in an intracontinental setting. Geology 33, 465–468.

Wood, D.A., Gibson, I.L. and Thompson, R.N., 1976. Elemental mobility during zeolite facies metamorphism of the Tertiary basalts of eastern Iceland. Contributions to Mineralogy and Petrology 55, 241-254.

794 Woodhead J., Eggins S., and Gamble J. (1993) High field strength and transition element
795 systematics in island arc and back-arc basin basalts: Evidence for multi-phase
796 extraction and a depleted mantle wedge. Earth Planet. Sci. Lett. **114,** 491–504.

797 Zegers, T.E., van Keken, P.E., 2001. Middle Archean continent formation by crustal
798 delamination. Geology 29, 1083–1086.

799

800

801

802 ## Figure captions

803 **Figure 1**

804 Simplified geological map of northern Tanzania (a) and the geological map of Geita
805 Greenstone Belt (b). SGB – Sukumalanad Greenstone Belt; NZ – Nzega Greenstone Belt; SM
806 – Shynianga-Malita Greenstone Belt; IS – Iramba-Sekenke Greenstone Belt; KF –
807 Kilimafedha Greenstone Belt; MM – Musoma-Mara Greenstone Belt. Inset map of Africa
808 showing the location of Archean blocks.

809 **Figure 2**

810 Geological map of the eastern part of the Geita Greenstone Belt showing the location of the
811 Kukuluma Intrusive Complex.

812 **Figure 3**

813 Photomicrographs showing the three main rock types found in the KIC. a and b) Medium
814 grained diorite; the mineralogy is dominated by amphibole (mostly actinolite) and plagioclase
815 with minor quartz. c and d) Medium grained monzonite; the mineralogy is dominated
816 plagioclase, k-feldspar, biotite and amphibole with minor quartz. The diorite and monzonite
817 have been deformed and metamorphosed to greenschist facies. As a result amphiboles and
818 pyroxenes have been partly replaced by actinolite. Note that the feldspars in both rock types
819 are not altered to sericite and appear fresh under microscope suggesting that the samples have
820 not been significantly affected by hydrothermal alteration. e and f) Photographs of a
821 porphyritic granodiorite dyke. Note that the feldspars from the granodiorite have been partly
822 replaced by sericite but appear mostly fresh under microscope. Small amounts of carbonate
823 and chlorite, disseminated or as microveins are present in all samples.

824

825 **Figure 4**

826 Series of diagrams showing that although the rocks of the KIC have been hydrated and
827 carbonated, as indicated by the petrography and LOI values, their major and trace element
828 composition was very little disturbed. In the alteration boxplot of Large et al. (2001) all
829 samples plot in the field of least altered rocks (a). Diagrams b and c show that there is no
830 correlation between the concentration of two of the most mobile major elements, Na_2O and
831 K_2O, and the LOI values. The same pattern is observed in d and e where the concentration of
832 two of the most mobile trace elements, Rb and Sr, are plotted against the LOI values
833 suggesting that most likely the concentration of these elements is close to their initial values.
834 The mobility of REE and HFSE was tested by plotting the values of La (f) and Nb (g) against
835 Zr, a highly immobile element. The good correlations suggest that these elements were most
836 likely immobile during post-magmatic alteration and metamorphism.

837 **Figure 5**

838 Major elements variation diagrams for the KIC. The grey area shows the field of sanukitoids
839 from Martin et al., (2010). The field of LSA (continuous line in Figure 5b) is from Castillo
840 (2012) and the field of basaltic experimental melts is from Rollison (1997) and Martin et al.,
841 (2005).

842 **Figure 6**

843 Chondrite normalized REE diagrams (a, c and e) and primitive mantle normalized trace
844 element diagrams (b, d and f) for the KIC rocks. Also shown is the average of LSA, HSA,
845 sanukitoids and Closepet-type granite from Martin et al., (2005).

846 **Figure 7**

847 Sr/Y vs Y (a) and La/Yb_n vs Yb_n (b) diagrams for the KIC samples. The field of LSA (ligh
848 grey) and HSA (darker grey) in (a) is from Castillo (2012) and the field of sanukitoids
849 (dashed line) is from Martin et al., (2005). The field of adakites in (b) is from Moyen and
850 Martin (2012). The diagrams in (c) and (d) show that the samples that have high Sr/Y (c) and
851 La/Yb_n ratios (d) also have high Dy/Yb_n ratio indicative of high pressure melting. The large
852 square (diorite suite) and the large circle (monzonite suite) show the samples with the highest
853 Mg# which also have the Sr/Y, La/Yb_n and Dy/Yb_n ratios. The line with arrow in (d) shows
854 that the interaction of eclogitic melts with the mantle peridotite leads to a decrease in the
855 La/Yb and Dy/Yb ratios in the melt (Kelemen et al., 2003).

856 **Figure 8**

857 Diagram (a) showing that at similar CaO values the monzonite suite has higher Na_2O which
858 may reflect clinopyroxene in the source and melting at higher pressure. The lack of
859 correlation (b) between the MgO and the Sr/Sr* suggest that the Sr anomaly is not the result
860 of plagioclase fractionation. (c) shows that Zr and Hf are fractionated from each other in the
861 monzonite suite which we attribute to residual rutile. The effect of residual rutile is shown in
862 (d) where the positive correlation between Nb/La and Zr/Sm ratios is indicative of residual
863 rutile (Münker et al., 2004). The dashed lines in (c) and (d) shows the chondritic ratios for the
864 respective elements while the arrows in (d) show the effect of residual rutile (positive
865 correlation) vs the effect of residual high-Mg amphibole (negative correlation).

866 **Figure 9**

867 Diagrams showing the compositional differences between LSA and HSA on K vs Rb (a), Sr
868 vs CaO+Na_2O (b) and Cr/Ni vs TiO_2 (c) compiled by Martin et al., (2005). In (a) the
869 continuous line shows the average K/Rb ratio in MORB (Sun and Mcdonough, 1989) while
870 the arrows show the effect of metasomatism, which increases the ratio and the effect of

partial melting, which decreases the ratio. In all three diagrams the KIC samples resemble more the HSA than the LSA and mostly overlap the field of experimental basaltic melts. The diagram in (d) show that there is no correlation between the Cr/Ni ratio and the Mg# indicating that the Cr/Ni ratio in the KIC samples is a source characteristic rather than the result of fractionation.

Figure 10

Diagram showing the variation of the Sr/Y ratio with MgO in modern arcs, Archean adakites and experimental melts from Chiaradia (2015). Chiaradia (2015) showed that in the modern arcs the Sr/Y ratio is a function of crustal thickness and the gradual increase of the Sr/Y ratio with increased crustal thickness also correlates with decreasing MgO suggesting that the Sr/Y ratio in modern arcs better reflects intracrustal processes than source characteristics. The sudden increase in Sr/Y ratios at low MgO in Archean adakites is similar to the data obtained for experimental basaltic melts and is consistent with partial melting of the lower mafic crust in the Archean. The KIC samples have Sr/Y and MgO values similar to the experimental basaltic melts and the Archean adakites suggesting lower mafic crust melting. The diagram in (b) shows that the diorite and the granodiorite suite have near MORB/chondritic Zr/Hf and Th/U ratios while the monzonite suite has Zr/Hf ratios similar to the mafic end member (mlc) of the lower crust (Hacker et al, 2015) and the Th/U ratio varies between the mafic end member of the lower crust and the lower continental crust (lcc) values of Rudnick and Gao (2003). However, the Th/U ratios in all samples are near chondritic suggesting that Th and U were not fractionated from each other as required by a subduction environment.

Element	LSA	HSA	Sanukitoid	Closepet	Monzonite suite	Diorite suite	Granodiorite	KIC (average)
SiO_2 (%)	56.25	64.80	58.76	56.39	56.41	58.61	62.50	57.51
TiO_2 (%)	1.49	0.56	0.74	1.20	0.49	0.51	0.55	0.50
Al_2O_3 (%)	15.69	16.64	15.80	15.79	15.70	16.09	15.69	15.90
FeO (%)	5.82	4.27	5.28	6.60	5.71	6.39	4.89	6.05
MnO (%)	0.09	0.08	0.09	0.13	0.07	0.08	0.08	0.07
MgO (%)	5.15	2.18	3.90	3.38	3.54	2.90	1.89	3.22
CaO (%)	7.69	4.63	5.57	5.45	4.99	4.58	3.71	4.79
Na_2O (%)	4.11	4.19	4.42	3.94	5.61	4.20	3.37	4.90
K_2O (%)	2.37	1.97	2.78	3.17	2.59	2.16	3.67	2.38
P_2O_5 (%)	0.66	0.20	0.39	0.72	0.50	0.22	0.16	0.36
K_2O/Na_2O	0.58	0.47	0.63	0.80	0.49	0.51	1.10	0.50
$CaO+Na_2O$	11.80	8.82	9.99	9.39	10.59	8.78	7.08	9.69
$FeO+MgO+MnO+TiO_2$	12.55	7.09	10.01	11.31	9.81	9.88	7.42	9.85
Y (ppm)	13.00	10.00	18.00	37.00	17.24	9.794	16.41	13.52
Yb (ppm)	0.93	0.88	1.32	2.05	1.18	0.85	1.57	1.02
Sr (ppm)	2051.00	565.00	1170.00	978.00	1128.38	834.34	331.96	981.36
Cr (ppm)	157.00	41.00	128.00	50.00	86.91	75.10	21.24	81.00
Ni (ppm)	103.00	20.00	72.00	38.00	46.65	53.00	13.43	49.83
Sr/Y	162.21	55.65	63.98	26.43	71.39	85.19	20.25	78.29
La/Yb	44.19	21.82	45.38	44.34	82.76	26.68	15.20	54.72
Mg#	0.61	0.48	0.57	0.48	0.53	0.46	0.41	0.49

Table 1. Table showing the average composition of the adakites, sanukitoids and Closepet-type granite (Martin et al., 2005) and the average composition of the Kukuluma Intrusive Complex rocks.

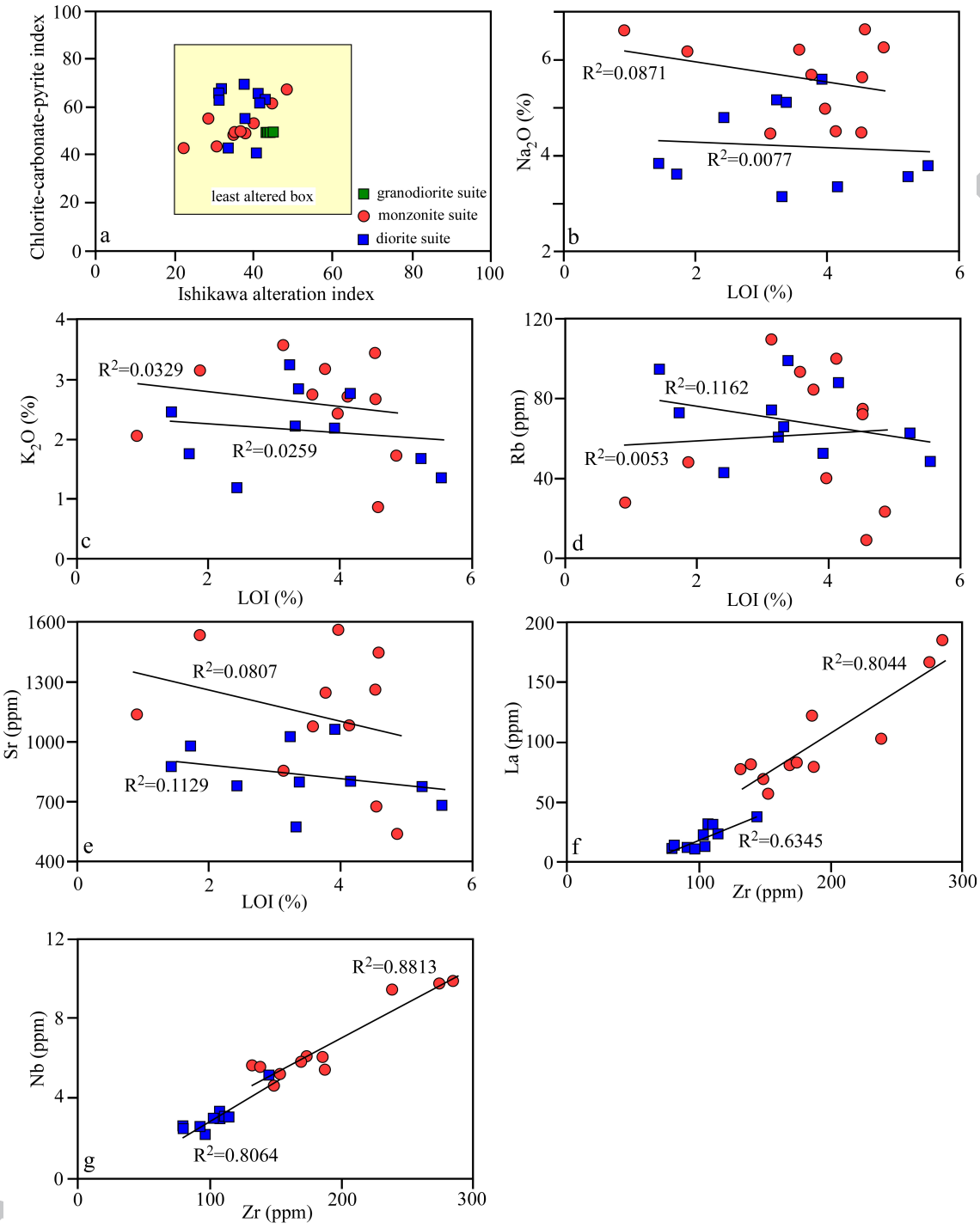

Figure 4

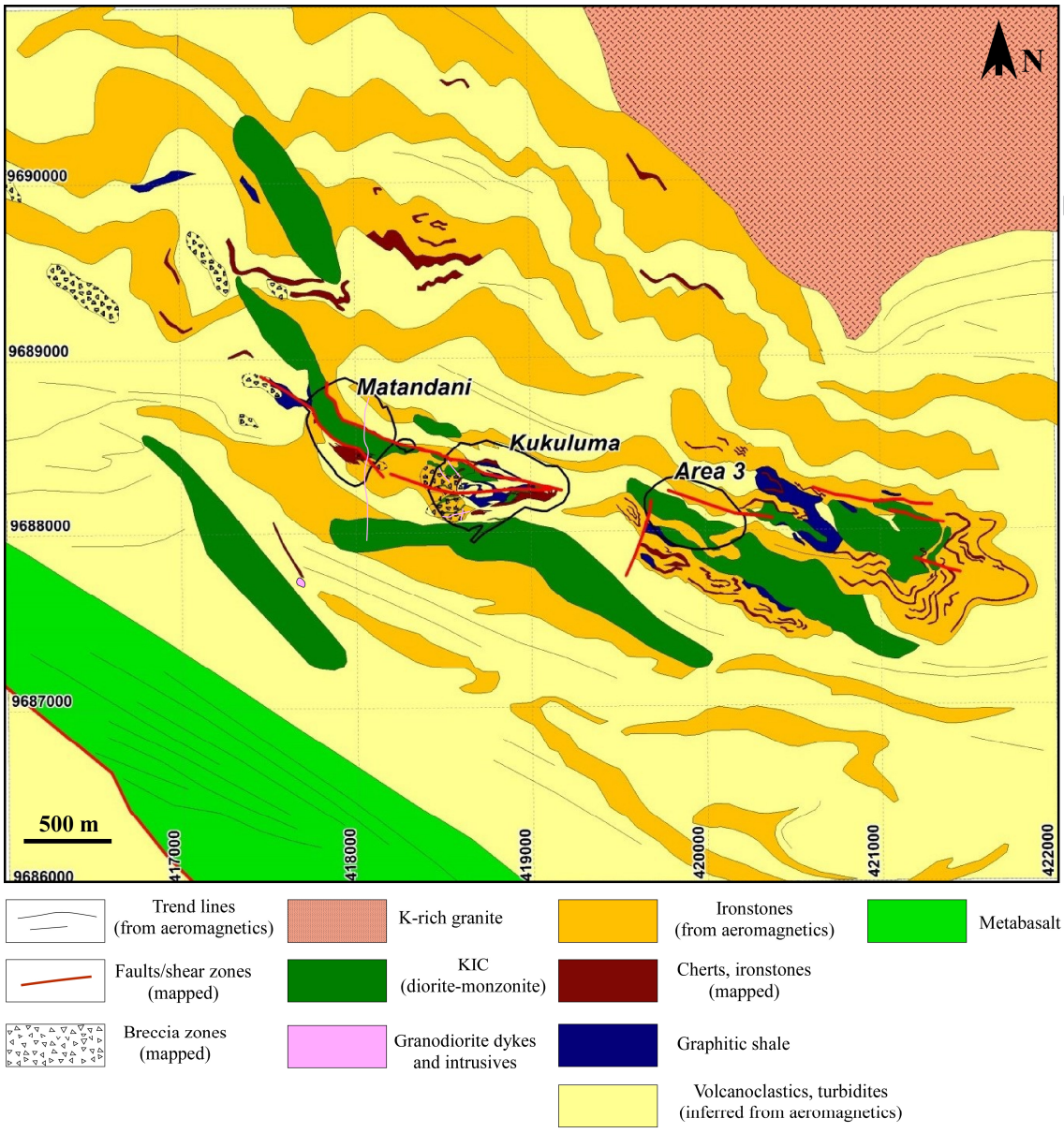

Figure 2

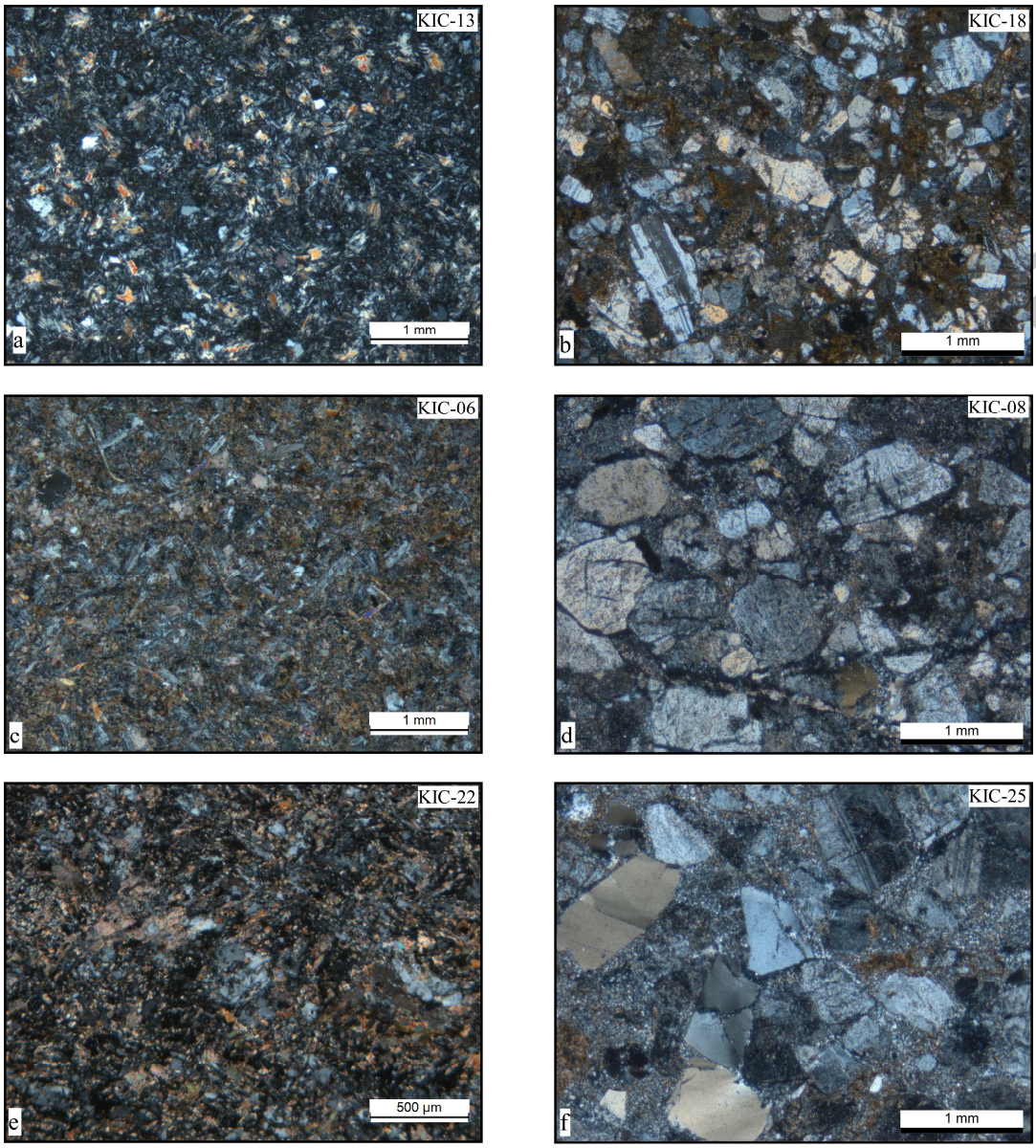

904 **Figure 3**

905

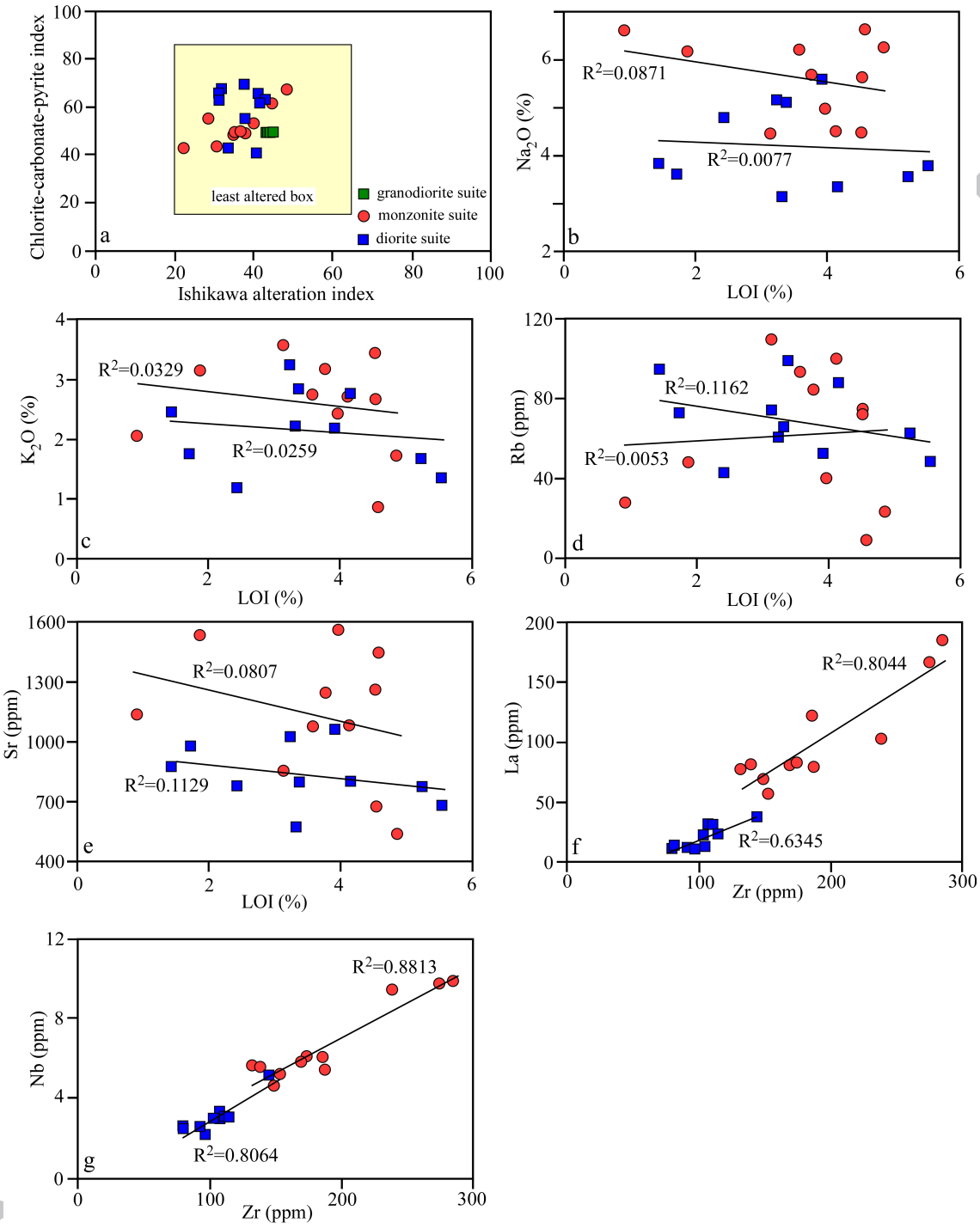

Figure 4

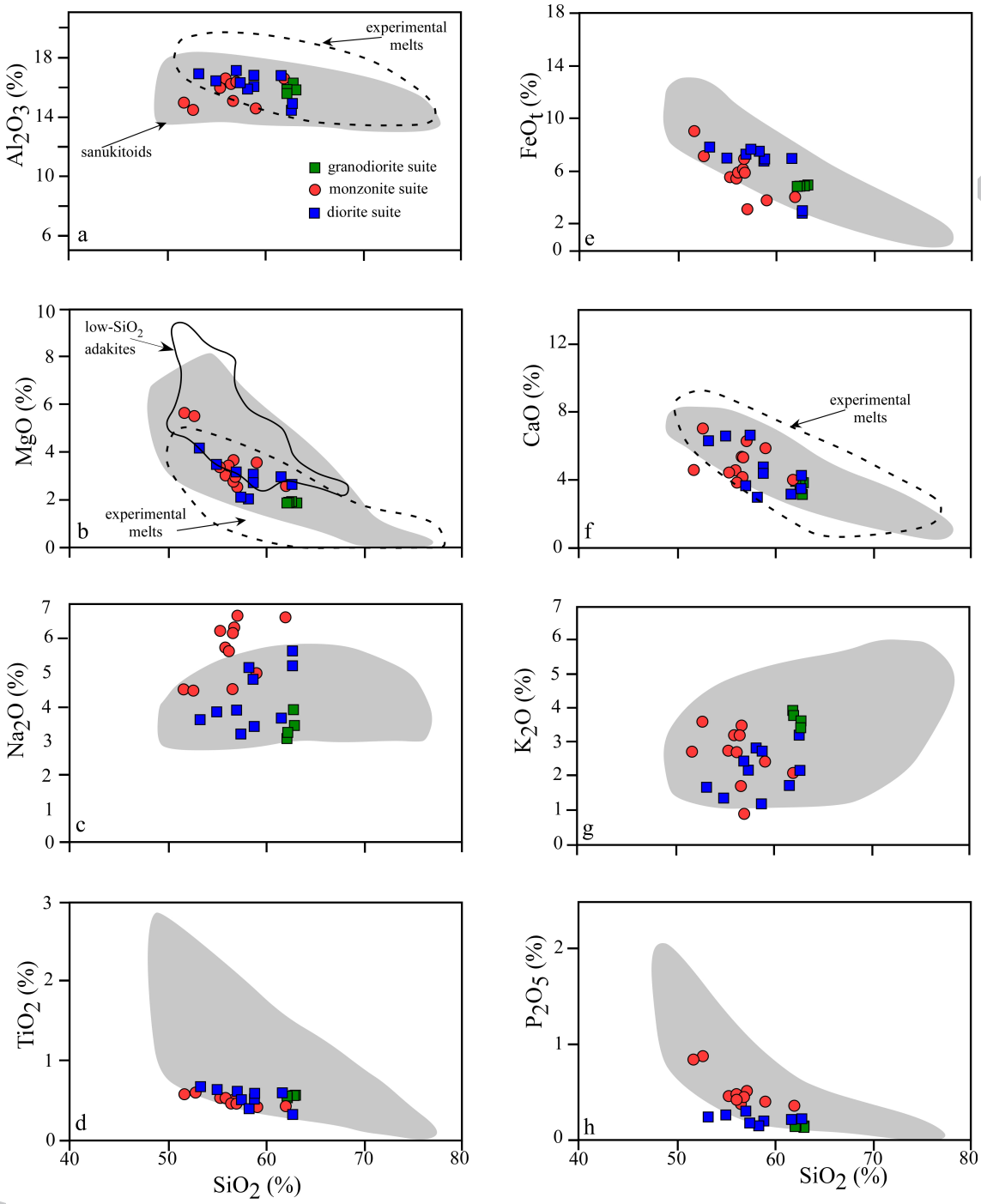

Figure 5

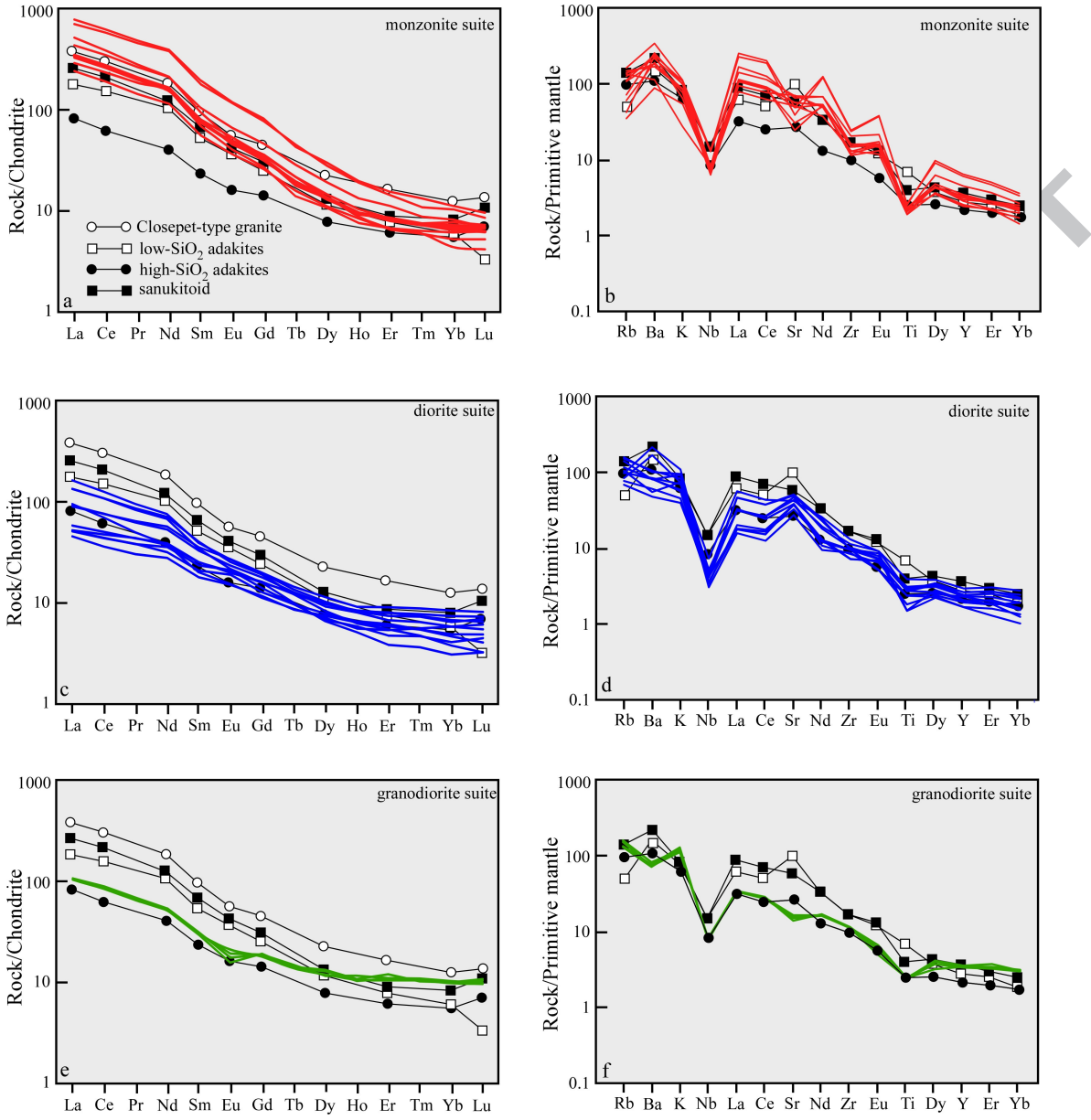

910 **Figure 6**

911

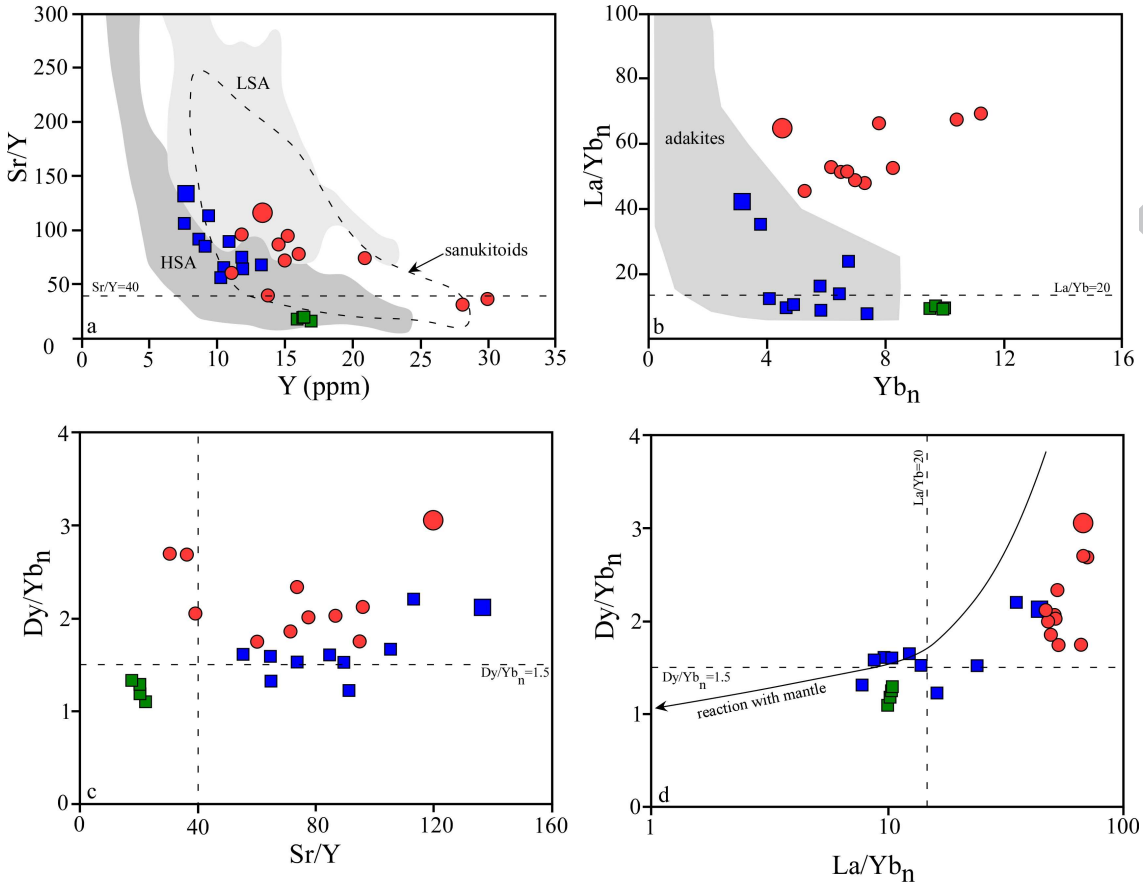

912 **Figure 7**

913

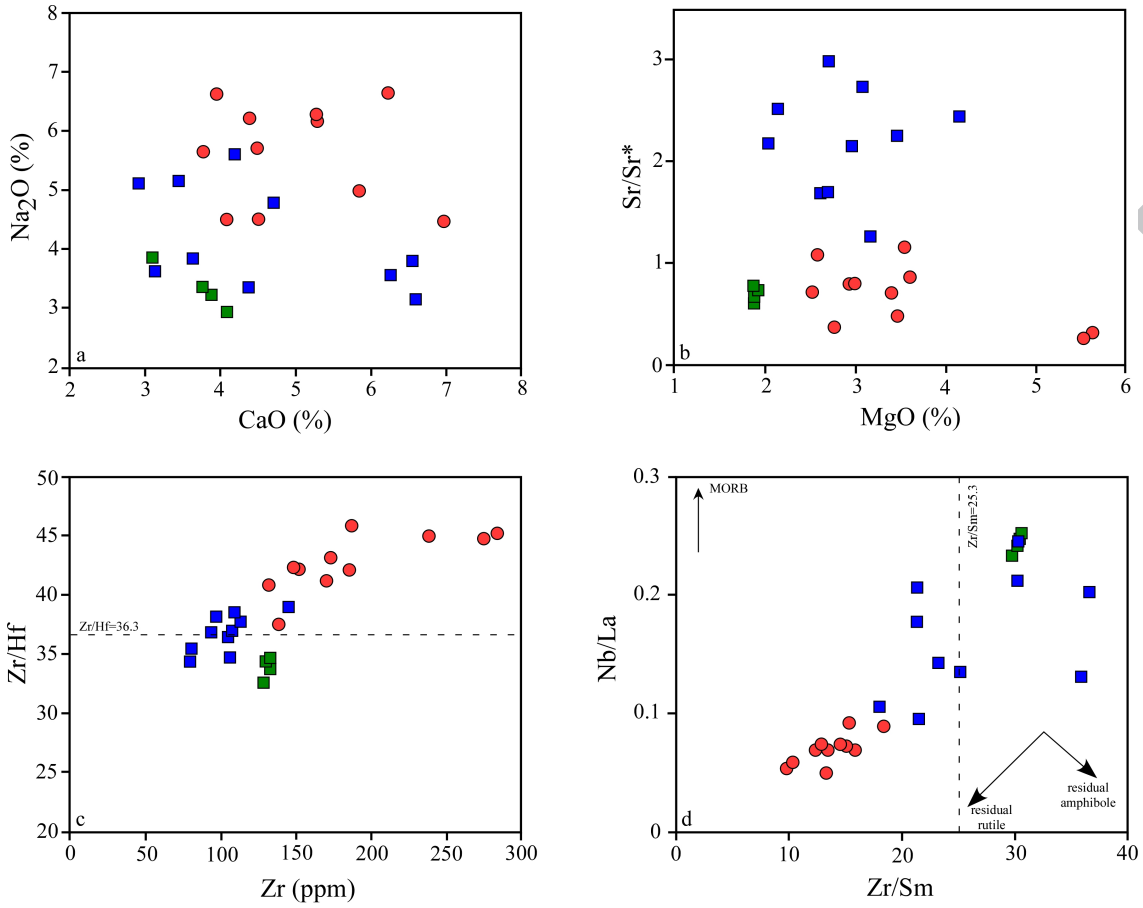

914 **Figure 8**

915

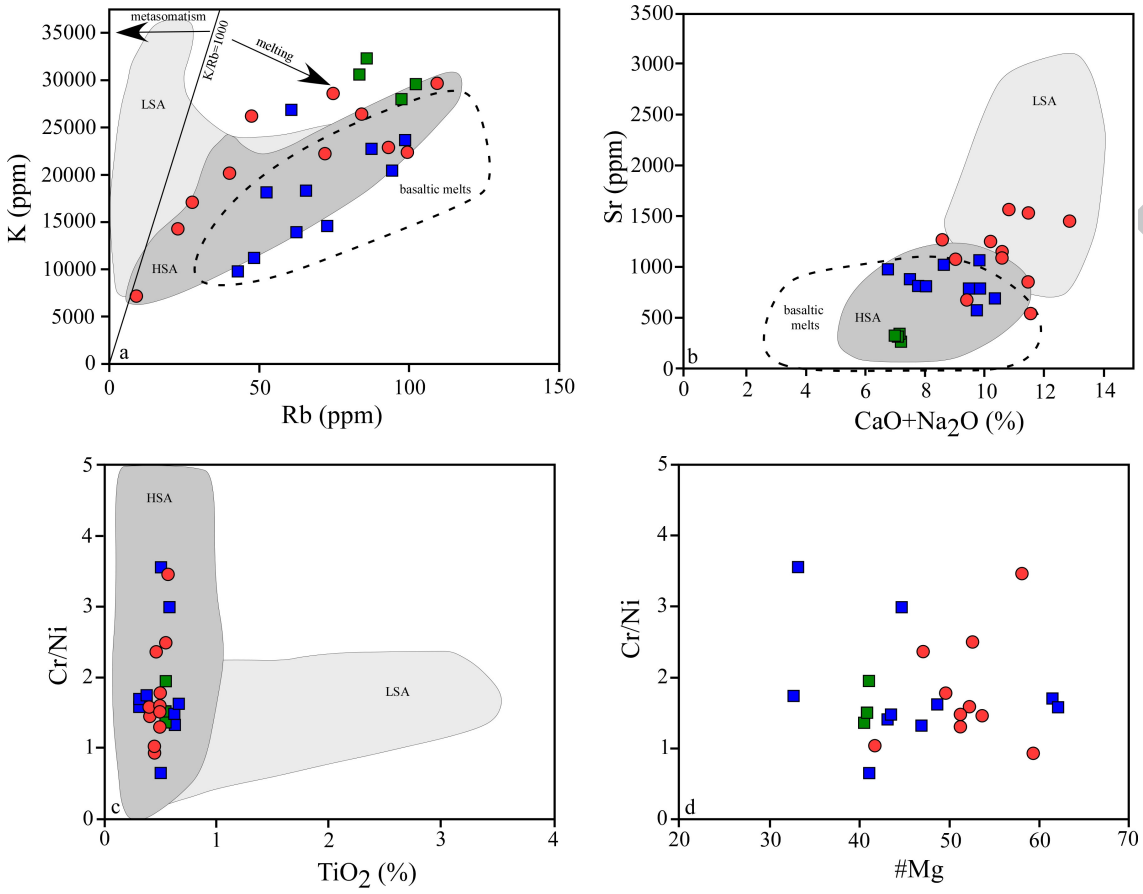

916 **Figure 9**

917

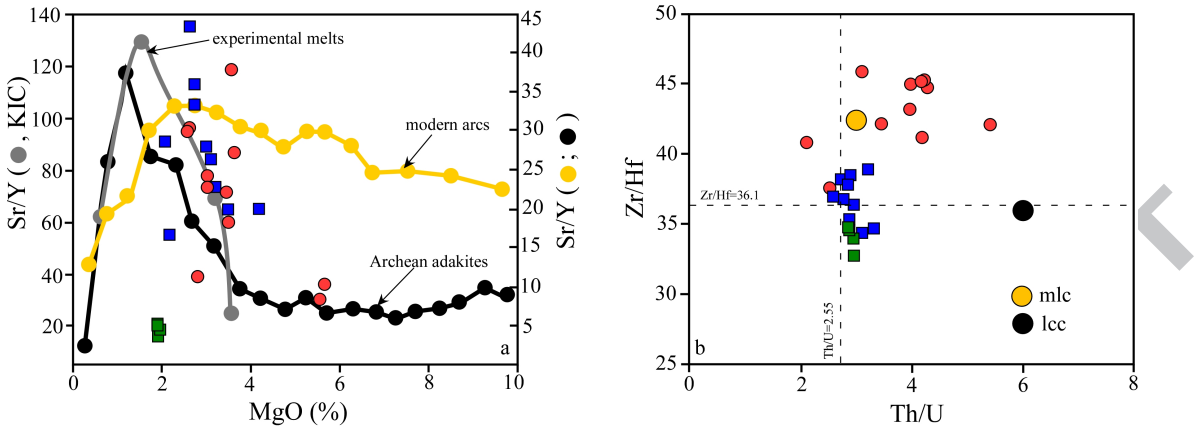

Figure 10

Highlights

- The KIC is a syn-tectonic Neoarchean igneous complex with intermediate composition
- The KIC has high Sr/Y and La/Yb ratios indicative of a melting in the garnet stability field
- The KIC formed by partial melting of thickened mafic/ultramafic lower crust
- The KIC is related to the removal of the eclogitised root of an oceanic plateau